Study of Self-Heating Effects in GaN HEMTs

by

Towhid Chowdhury

A Thesis Presented in Partial Fulfillment
of the Requirements for the Degree
Master of Science

Approved May 2013 by the
Graduate Supervisory Committee:

Dragica Vasileska, Chair
Stephen Goodnick
Michael Goryll

ARIZONA STATE UNIVERSITY

August 2013

ABSTRACT

GaN high electron mobility transistors (HEMTs) based on the III-V nitride material system have been under extensive investigation because of their superb performance as high power RF devices. Two dimensional electron gas(2-DEG) with charge density ten times higher than that of GaAs-based HEMT and mobility much higher than Si enables a low on-resistance required for RF devices. Self-heating issues with GaN HEMT and lack of understanding of various phenomena are hindering their widespread commercial development. There is a need to understand device operation by developing a model which could be used to optimize electrical and thermal characteristics of GaN HEMT design for high power and high frequency operation.

In this thesis work a physical simulation model of AlGaN/GaN HEMT is developed using commercially available software ATLAS from SILVACO Int. based on the energy balance/hydrodynamic carrier transport equations. The model is calibrated against experimental data. Transfer and output characteristics are the key focus in the analysis along with saturation drain current. The resultant IV curves showed a close correspondence with experimental results. Various combinations of electron mobility, velocity saturation, momentum and energy relaxation times and gate work functions were attempted to improve IV curve correlation. Thermal effects were also investigated to get a better understanding on the role of self-heating effects on the electrical characteristics of GaN HEMTs. The temperature profiles across the device were observed. Hot spots were found along the channel in the gate-drain spacing. These preliminary results indicate that the thermal effects do have an impact on the electrical device characteristics at large biases even though the amount of self-heating is underestimated with respect to

thermal particle-based simulations that solve the energy balance equations for acoustic and optical phonons as well (thus take proper account of the formation of the hot-spot). The decrease in drain current is due to decrease in saturation carrier velocity. The necessity of including hydrodynamic/energy balance transport models for accurate simulations is demonstrated. Possible ways for improving model accuracy are discussed in conjunction with future research.

Dedicated to my beloved parents

ACKNOWLEDGMENTS

Several individuals played an important role whose sincere help made me complete this thesis. I would first like to thank Professor Dr. Dragica Vasileska for her ample support in giving direction to my research, keeping the thesis on track, ensuring the quality of final result and helping me in exploring the exciting challenging world of TCAD simulations. I would like to thank my Graduate Supervisory Committee members Professor Dr. Stephen M. Goodnick and Professor Dr. Michael Goryll for providing me useful information regarding my research. Late Dr. Dieter Schroder had helped me develop a better understanding of device physics theory by always being readily available to answer my questions. He has been also an inspiration for me to take up the field of solid state devices as a field of career. I would like to thank the group members of Professor Dr. Dragica Vasileska in providing guidelines to edit my thesis and also provide stimulating discussions on the physics of the device(Balaji Padmanabhan).

I thank my parents for their devotion in raising me and being a great support for me all during these several months of hard work.

TABLE OF CONTENTS

Page

CHAPTER Page

CHAPTER Page

LIST OF TABLES

LIST OF FIGURES

Figure Page

Figure Page

Chapter 1 INTRODUCTION

1.1. Overview

Silicon technology has dominated the semiconductor device industry with its established CMOS process since 1960s[1].But there are some applications like Light Emitting Diodes, Radio Frequency (RF) devices and high-temperature and high-power electronic devices where III-V nitrides compound semiconductor have attracted intense interest[2-4].Power amplifiers are key elements for applications like phased array radar and base stations. AlGaN/GaN high electron mobility transistors (HEMTs) offer important advantages for high power applications due to GaN large bandgap and high breakdown electric field[5].High power microwave circuits have already been proposed showing the great prospect of this technology. Table 1.1 shows a comparison of the important material properties of GaN and other conventional semiconductors.

Table 1.1- Semiconductor material properties at 300K

Property	Si	GaAs	SiC	GaN
Bandgap(eV)	1.12	1.42	3.25	3.40
Breakdown field(MV/cm)	0.25	0.40	3.0	4.0
Electron mobility (cm^2/Vs)	1350	6000	800	1300
Maximum velocity(cm/s)	1.0	2.0	2.0	3.0
Dielectric constant	11.8	12.8	9.7	9.0

In addition to large bandgap that leads to large breakdown field, the polar nature of GaN crystal between the top layer (AlGaN) and that in the bottom layer (GaN)gives it an advantage over other materials. This polarization is due to the bulk properties with asymmetric lattice structure and strain in one or both layers. This leads to much higher sheet carrier densities than conventional GaAs/AlGaAs heterostructures. The typical charge density is about 2×10^{13} cm^{-2},which is about ten times higher than what can be achieved in AlGaAs/GaAs HEMTs[6-9].This results in>10× power performance from GaAs and Si structures[10].

With all the remarkable promises which GaN shows, the reliability of such devices is still an issue. The overall power present in GaN based HEMTs is large and cannot be totally dissipated through the substrate. As a result, AlGaN/GaN HEMTs suffer from self-heating effects. Self-heating is one of the critical factors that reduces device lifetime and reliability as channel temperature can reach several hundred degrees above ambient base temperature. Severe self-heating effect may deteriorate the gate electrode and can burn metal wires connecting the chip to the package, and hence result in device failures and reliability issues[11–12].The study of reliability of GaN HEMTs and the knowledge of heat dissipation in these transistors is crucial to develop a stable technology.

Computer modeling has proven to be a versatile tool for engineering design and analysis. Nowadays, the Silvaco software, which is a Technology Computer Aided Design (TCAD) program, has been extensively used for design and analysis of semiconductor devices and processes. This thesis discusses the physics of self -heating by

performing numerical simulation using Silvaco. Numerical simulation is a good way to develop understanding of device physics operation by creating a model of the real device that incorporates various physical phenomena. It can be used to compare and predict experimental output for different combination of voltages, doping levels etc. It also saves a lot of device fabrication cost as fewer number of devices need to be fabricated in the design and test process.

1.2. History of GaN devices

Group III-nitrides have shown a great prospect for realizing optoelectronic devices and other type of devices particularly HEMT. Of the Group-III nitrides, Johnson *et al*. [13]first synthesized GaN in 1928 as small needles and platelets. In 1969, Maruska and Tietjen[14]found out that the undoped GaN crystals have very high inherent doping, typically up to 10^{19} cm^{-3} due to the high density of nitrogen vacancies. They grew the first single crystal film of GaN on the sapphire substrate[15] which initiated the first GaN research for semiconductor devices (initially for bulk GaN) in the 1960s, and then for the improvement of the epitaxial growth techniques in the 1980s.

In the late 1980s, Amano *et al*. reported that high quality GaN films could be obtained by a two-step process, which used an AlN buffer layer before GaN deposition [16] (Figure 1.1). This paved the way for significant improvement of both the crystal structure and electrical properties of GaN over the next few years. In 1989, the p-type doping problem was solved by post-growth low-energy electron beam irradiation treatment of Mg-doped

GaN. Nakamura *et al*. replaced this process by a post growth thermal treatment. The first AlGaN/GaN hetero-junction was reported by Khan *et al*.[17] with a carrier density of 10^{11} cm^{-2} and a mobility of 400-800 cm^2/Vs. This was the first group to report the DC and RF behavior of GaN HEMTs in 1993 and 1994 respectively[18,19]. The saturation drain current of 40 mA/mm was achieved with a gate length of 0.25 µm. A power density of 1.1 W/mm at 2 GHz was achieved by Wu *et al*. in 1996[20]. These early HEMTs exhibited poor performance in terms of transconductance and frequency response. As the crystal quality improved, the transconductance, current capacity, and frequency response increased, and presently GaN HEMTS are one of the leading candidates for high power and high frequency device applications. Metal-organic chemical vapor deposition(MOCVD) and molecular beam epitaxy(MBE) are now the leading growth technologies for depositing these high quality GaN heterostructure-based devices. Optimization of the MOCVD growth of GaN-based quantum structures has enabled high efficiency blue LEDs and laser diodes to be achieved. GaN-based blue and green LEDs with external quantum efficiencies of 10% and 5 mW output power at 20 mA have been demonstrated recently.

To further improve the performance of GaN HEMTs, SiN passivation layer is deposited on top of GaN substrate using lateral epitaxial growth technique which has proven to be extremely effective in reducing DC to RF dispersion[21]. Using this technique, small windows are etched through to the underlying GaN film. The GaN film eventually grows

laterally over the mask and this film is defect free since the threading dislocations are present only in the growth direction through the windows and not the lateral direction[22].

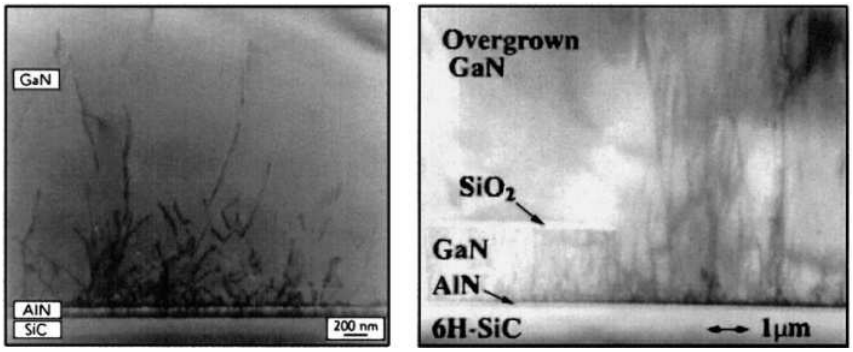

Figure 1.1 TEM crosssection of MOCVD grown GaN on SiC substrate using AlN buffer layer (left) and LEO grown GaN (right)[22].

Another improvement on the operation of GaN HEMTs (used to increase the break-down voltage)has been made with the inclusion of field plates. The field plate technique is diagramed in Figure 1.2[24].It was first implemented on a GaN HEMT by Chini. This technique greatly reduced drain current dispersion, avoiding the 'knee walk-out' phenomena shown in Figure 1.3 as gate voltage is increased[25].

In summary, in the last decade and half, the performance of GaN HEMT has improved significantly.

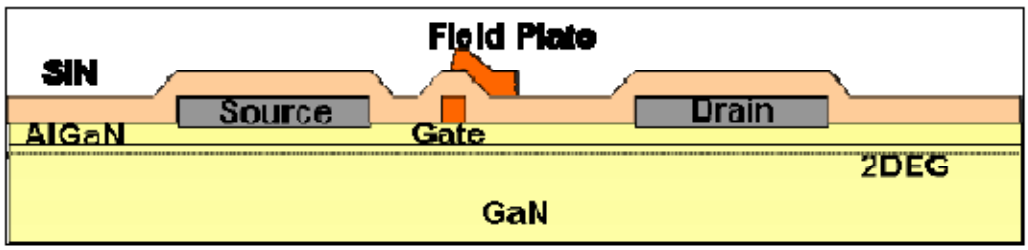

Figure 1.2. Field- Plated Device Structure[24] .

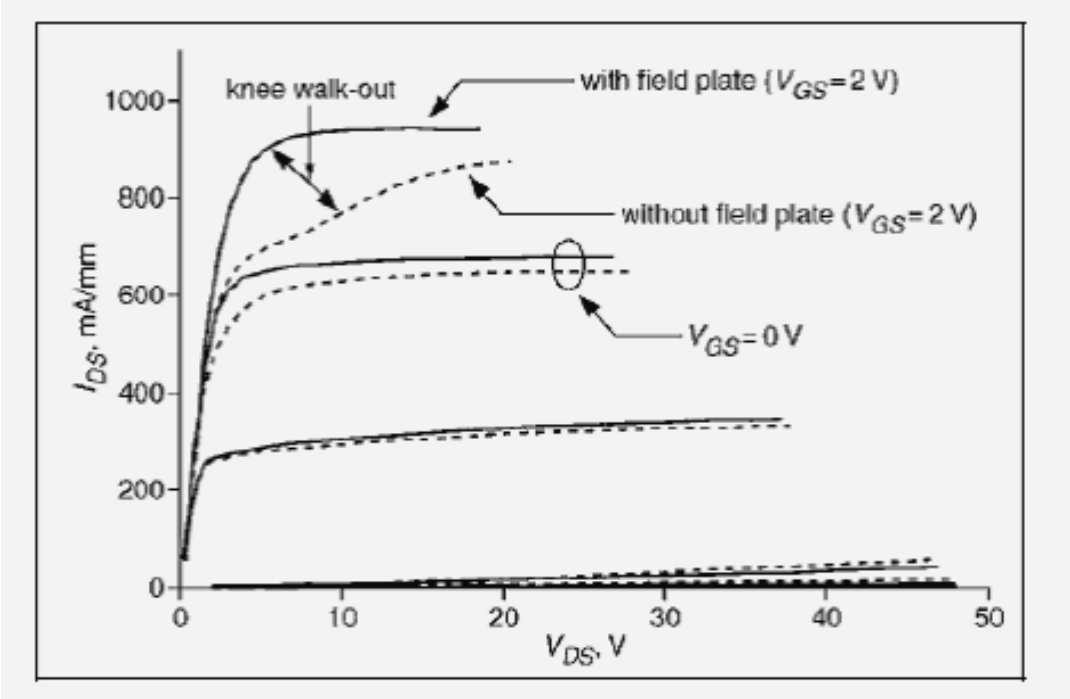

Figure 1.3 IV characteristics showing knee walk-out[25].

1.3. Piezoelectric and Spontaneous Polarization

In GaN based heterostructures, the main reason behind the accumulation of carriers at the hetero-interface is inherent net polarization. GaN based materials poses an inherent spontaneous polarization P_{SP} whose direction depends on the growth face of the crystal (Ga or N at the face).In addition to spontaneous polarization, the strain developed at the crystal leads to piezoelectric polarization P_{PE}. When AlGaN is grown over the GaN substrate, due to difference in their polarization, a net polarization charge develops at the interface depending on the face of growth of the crystal. In the case of GaN, a basal

surface should be either Ga- or N-faced. It is, however, important to note that the (0001) and $(000\bar{1})$ surfaces of GaN are nonequivalent and differ in their chemical and physical properties[26].Figure 1.4 shows the crystal structure of wurtzite Ga-face and N-face GaN.

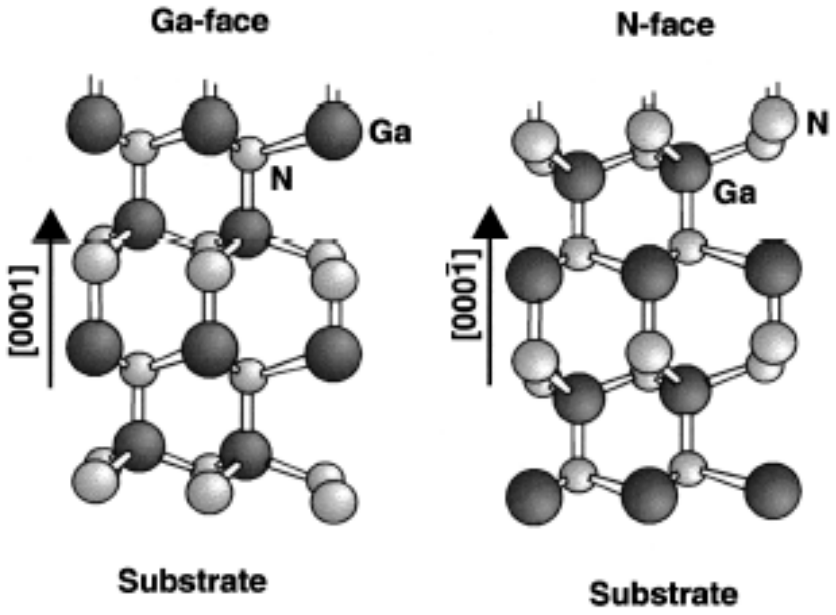

Figure 1.4 Crystal structure of wurtzite Ga-face and N-face Gallium Nitride[26].

The HEMT structures are generally grown along the c-axes and the spontaneous polarization along the axes is given by,

$$P_{sp} = P_{sp}z \tag{1.1}$$

The piezoelectric polarization charge is evaluated by,

$$P_{PE} = e_{33}\varepsilon_z + e_{31}(\varepsilon_x + \varepsilon_y) \tag{1.2}$$

where, e_{33} and e_{31} are piezoelectric coefficients.Here,

$$\varepsilon_z = \frac{c - c_0}{c_0} \tag{1.3}$$

where, ε_z is the strain along the c axis and the strain in the plane perpendicular to the c-axis is:

$$\varepsilon_x = \varepsilon_y = \frac{a - a_0}{a_0} \tag{1.4}$$

The amount of piezoelectric polarization in the direction of the c axis can, thus, be determined by

$$P_{PE} = 2\frac{a - a_0}{a_0}\left(e_{31} - e_{33}\frac{C_{13}}{C_{33}}\right) \tag{1.5}$$

where C_{13} and C_{33} are elastic constants. The piezoelectric polarization of AlGaN comes out to be negative for tensile and positive for compressive strained barriers, respectively. The spontaneous polarization for both GaN as well as AlN are found to be negative and hence, for Ga(Al)-face heterostructures the spontaneous polarization will point towards the substrate. The alignment of the piezoelectric and spontaneous polarization is parallel in the case of tensile strain, and anti-parallel in the case of compressively strained top layers as shown in Figure 1.5. If the polarity changes from Ga-face to N-face material, the piezoelectric and spontaneous polarization changes its sign (Figure 1.5).

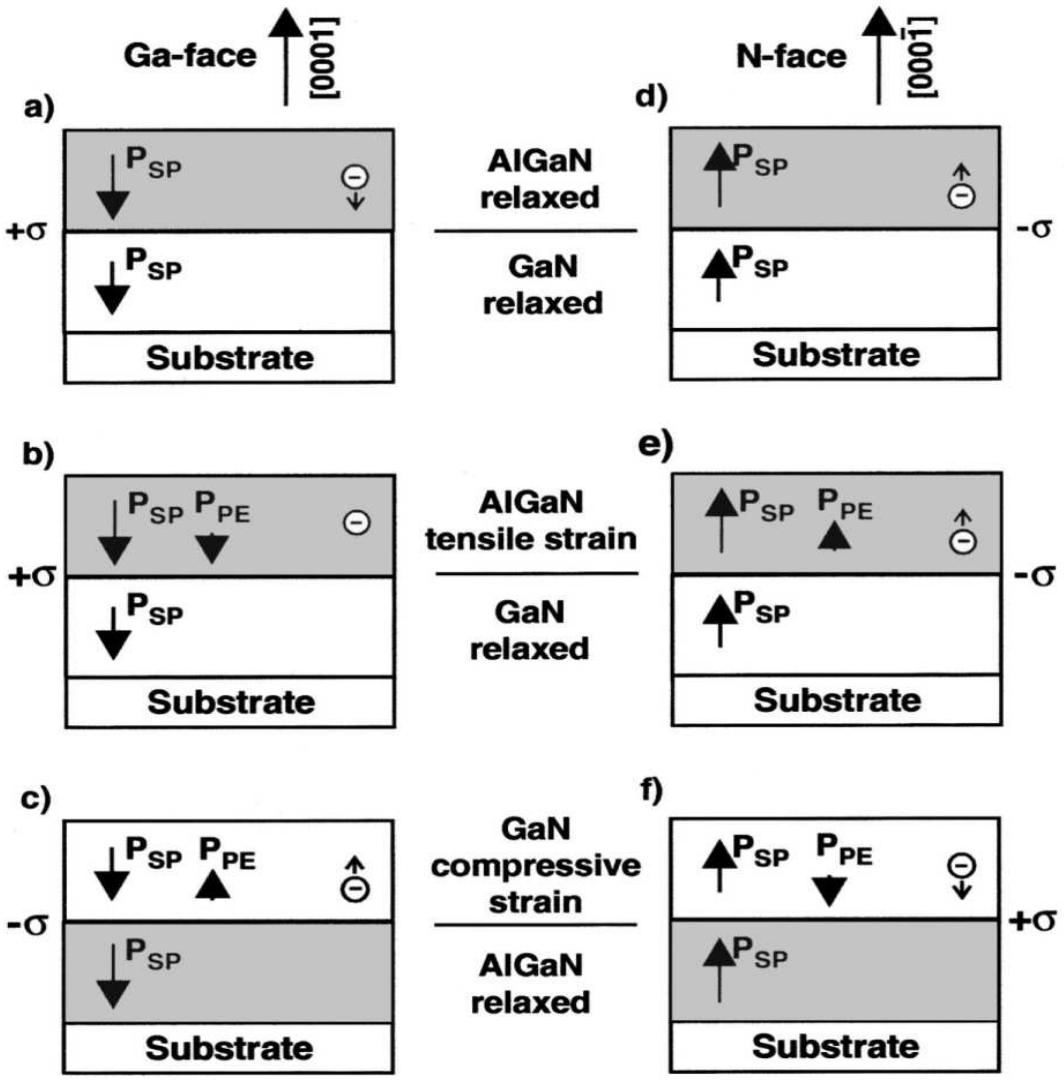

Figure 1.5 –Spontaneous and Piezoelectric polarization charge and their direction in Ga-faced and N-faced strained and relaxed AlGaN/GaN HEMT [26].

The effective polarization charge at any interface is given by,

$$\rho_P = \nabla P \qquad (1.6)$$

where, ρ_P is the polarization induced charge density.

$$\sigma = P(\text{Top}) - P(\text{Bottom}) \tag{1.7}$$

$$\sigma = [P_{SP}(\text{Top}) + P_{PE}(\text{Top})] - [P_{SP}(\text{Bottom}) + P_{PE}(\text{Bottom})] \tag{1.8}$$

where, σ is the polarization sheet charge density.

The polarization induced sheet charge density is positive in pseudomorphically grown AlGaN/GaN heterostructures and free electrons will tend to compensate the polarization induced charge, thereby forming a two dimensional electron gas (2DEG) at the AlGaN/GaN interface. A negative sheet charge density will accumulate holes at the interface. The following set of linear interpolations between the physical properties of GaN and AlN are utilized to calculate the net polarization induced sheet charge density σ at the AlGaN/GaN as a function of the Aluminum mole fraction *x* of the $Al_xGa_{1-x}N$ barrier[26].

Lattice constant:

$$a(x) = (-0.077x + 3.189)10^{-10}\,\text{m} \tag{1.9}$$

Elastic constants:

$$c_{13}(x) = (5x + 103)\text{GPa} \tag{1.10}$$

$$c_{33}(x) = (-32x + 405)\text{GPa} \tag{1.11}$$

Piezoelectric constants:

$$e_{31}(x) = (-0.11x - 0.49)\text{C} / \text{m}^2 \tag{1.12}$$

$$e_{33}(x) = (0.73x + 0.73)C / m^2 \quad (1.13)$$

Spontaneous polarization:

$$P_{SP}(x) = (-0.052x - 0.029)C / m^2 \quad (1.14)$$

The GaN substrate is thick and therefore is not strained. Thus, its piezoelectric component of polarization charge is taken as 0 C/m^2.Therefore, the effective polarization charge at the AlGaN/GaN interface is given by,

$$\left|\sigma(x)\right| = \left|P_{PE}(Al_xGa_{1-x}N) + P_{SP}(Al_xGa_{1-x}N) - P_{SP}(GaN)\right| \quad (1.15)$$

since,

$$\sigma = P(Top) - P(Bottom) \quad (1.16)$$

The absence of stress along the growth direction helps us to represent the strain in the z direction as,

$$\varepsilon_z = -2\frac{c_{13}}{c_{33}}\varepsilon_x + \frac{e_{33}}{c_{33}}E_z^{AlGaN} \quad (1.17)$$

where, E_z^{AlGaN} is the electric field in the AlGaN layer.

1.4. Thermal Issues of AlGaN/GaN HEMTs

Although the GaN based devices have the advantage of high electron density and output current, the high current flow generates a lot of heat which is known as self-heating. Self-heating is a serious concern in GaN devices. Due to self-heating, channel temperatures can reach several hundred degrees above the ambient base temperature. The

temperature increases can significantly change the temperature dependent material properties like band-gap and mobility which lead to degradation of device performance. The reduction in mobility leads to a reduction in current due to increased operating voltage. This decreases the maximum power density and also increases the gate leakage. Figure 1.6 shows the dependence of mobility on sheet carrier concentration. Mobility values at all temperatures reduce to same value for very high sheet concentration ($>10^{20}$ cm^{-3}). For small sheet carrier concentration the lower the temperature the higher the carrier mobility[27].The dependence of the carrier mobility upon the temperature for three different sheet carrier concentrations n_s is shown in Figure 1.7.

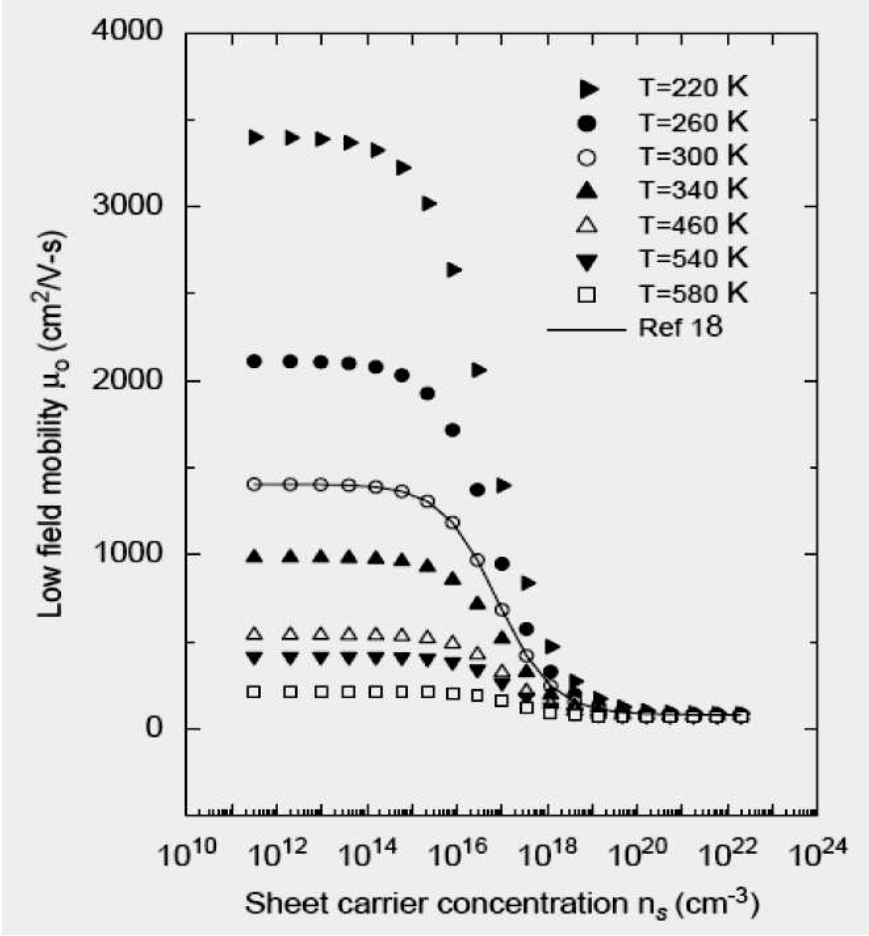

Figure 1.6. Low-field mobility μ_o (cm^2/Vs)variation with sheet carrier concentration n_s(cm^{-3})[27]

Table 1.2 lists the mobility values and the corresponding temperature at $n_s=10^{11}$ cm^{-3}.

Table 1.2 Mobility and the corresponding temperature

Temperatue(K)	220	260	300	340	460	540	580
Mobility(cm^2/Vs)	3392	2112	1405	983	538	415	107

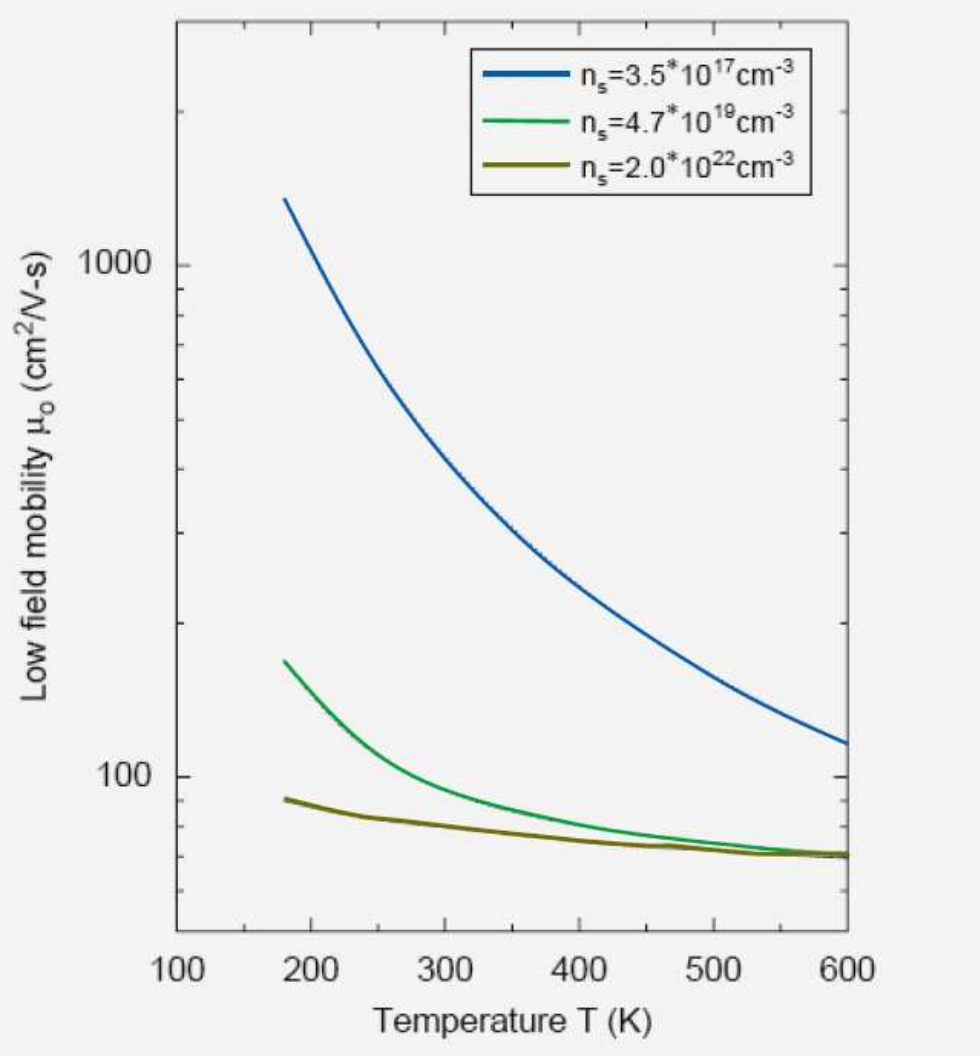

Figure1.7. Dependence of low-field mobility μ_o (cm^2/Vs) on temperature T(K)[27].

The amount of self-heating also depends upon the thermal conductivity of the substrate that is used. Popular substrate materials currently used for GaN HEMTs include sapphire, Silicon Carbide (SiC), silicon (Si) and Aluminum Nitride (AlN).Each substrate choice

has been proven with individual successes.

- Sapphire(Al_2O_3) had been a popular choice for substrate material due to its high melting point and ready availability. GaN purity levels are affected during vapor growth by the interaction of hydrogen gas and the oxygen in sapphire, creating unwanted defects, thus limiting the mobility. The thermal conductivity of sapphire has also been a limiting factor[28].
- Pure silicon has been used quite successfully as a substrate material for GaN HEMTs. Thermal conductivity of Si is similar to that of GaN. High purity silicon is readily available. However, lattice mismatch requires the use of a nucleation layer, further increasing the channel distance from the thermal management substrate [29].
- SiC has been a popular choice for high-power HEMT use providing a much higher thermal conductivity. But defects in SiC have made GaN layer growth difficult as the structure struggles to maintain uniformity during the crystal growth process [28]. AlN is often used as a nucleation layer between silicon based substrates and GaN to allow for lattice matching.
- As a free standing substrate, AlN has shown some promise as a GaN HEMT substrate choice but its thermal conductivity is only equal to that of sapphire.
- Bulk GaN substrate can eliminate trapping defect. But the thermal conductivity of GaN is a challenge to overcome which can lead to loss of linearity and device breakdown. While able to support high temperature

operation, GaN by itself is unable to sufficiently remove the heat generated during device operation.

- Diamond, which has the best thermal conductivity, is an option for GaN HEMT devices.

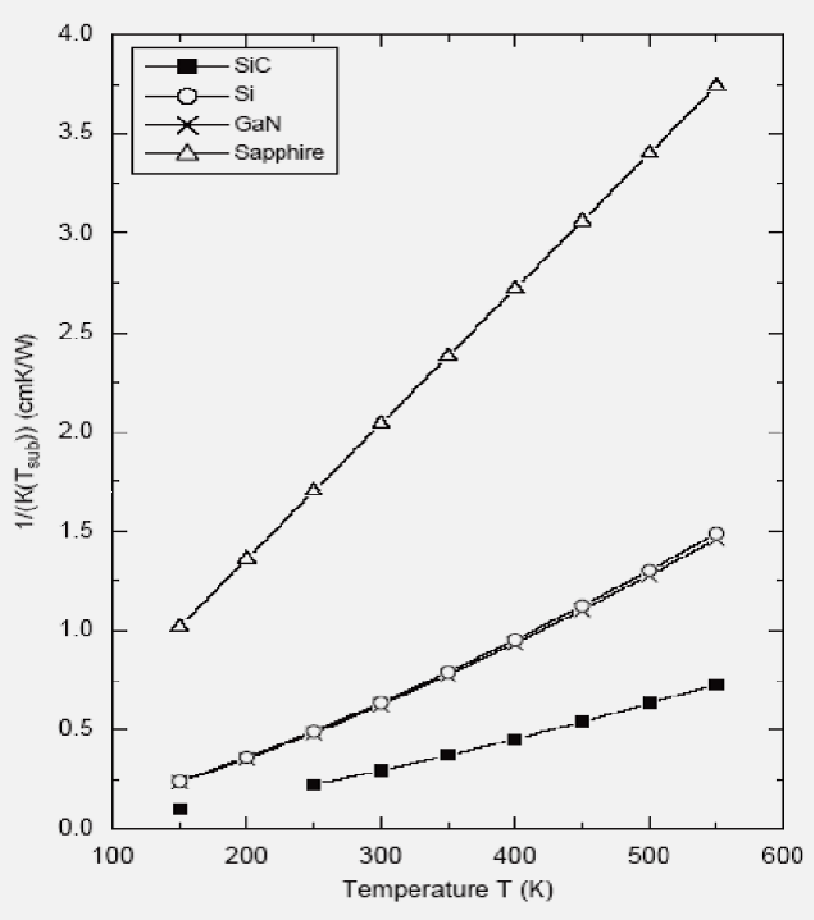

Figure 1.8 Inverse thermal conductivity $1/K(T_{sub})$ (cm K/W) variation with temperatureT(K) for different substrate materials[27].

The GaN HEMT with best power performance till now has been grown on SiC. Figure 1.8 presents the temperature dependence of inverse of the thermal conductivity(1/K) of various materials that can be used as substrates in AlGaN/GaN HEMTs. If the total epilayer thickness in the devices is significantly smaller than the device length, the thermal conductivity of the substrate plays a significant role in determining the temperature distribution profile in the epilayer structure and the heat dissipation from the active region of the device [27].

Table 1.3 Thermal conductivities of popular substrate materials.

Substrate	**Thermal conductivity(W/cm.K)**
Diamond	10
Sapphire	1.7
GaN	1.3
AlN	1.7
SiC	4.9
Si	1.5

1.5. Motivation for This Work and the Approach Pursued

The ultimate goal of this work is to develop a TCAD computer model within the Silvaco simulation framework for modeling of the characteristics of GaN HEMTs that allows one to examine the variation of the device performance with the inclusion of the polarization effects and thermal effects. In this simulation, hydrodynamic/energy balance transport model was used to simulate DC IV data of a GaN HEMT grown on GaN material. Joule heating model was introduced to model self-heating effects. Simultaneous

understanding the thermal and electrical properties of the GaN HEMTs allows for better optimization of the GaN transistor structure and prediction of thermal conductivity across layer interfaces.

Chapter 2 discusses the modeling approach used in Silvaco for analyzing the operation of GaN HEMTs. Chapters 3 presents important results for the different device simulations (with and without the inclusion of some of the effects studied), and summarizes the influence that these effects have on the device characteristics. Chapter 4 summarizes the results of this work and also provides thoughts on the scope for future research work.

Chapter 2 DEVICE MODELING AND SIMULATION

2.1. Semiconductor Device Simulations

Semiconductor device simulations provide in depth understanding of actual operations of solid state devices while at the same time reducing the computational burden so that the results can be obtained within a reasonable time frame.

2.1.1. Importance of Simulation

The semiconductor Industry has developed device simulations tools to reduce costs for R&D and production facilities. Semiconductor device modeling creates models for the behavior of the electrical devices based on fundamental physics. It may also include the creation of compact models which represent the electrical behavior of such devices but do not derive them from underlying physics. Device modeling offers many advantages such as: providing in-depth understanding, providing problem diagnostics and decreasing design cycle time. Simulations require enormous technical expertise not only in simulation techniques and tools but also in the fields of physics and chemistry. The developer of simulation tools needs to be closely related to the development activities in the research and commercial productions in industry.

2.1.2. General Device Simulation Framework

Figure 2.1 shows the main components of semiconductor device simulations at any level. It all begins with the electronic properties of solid state materials. The two

main kernels, transport equations that governed charge flows and electromagnetic fields that drive charge flows, must be solved self-consistently and simultaneously due to their strong coupling.

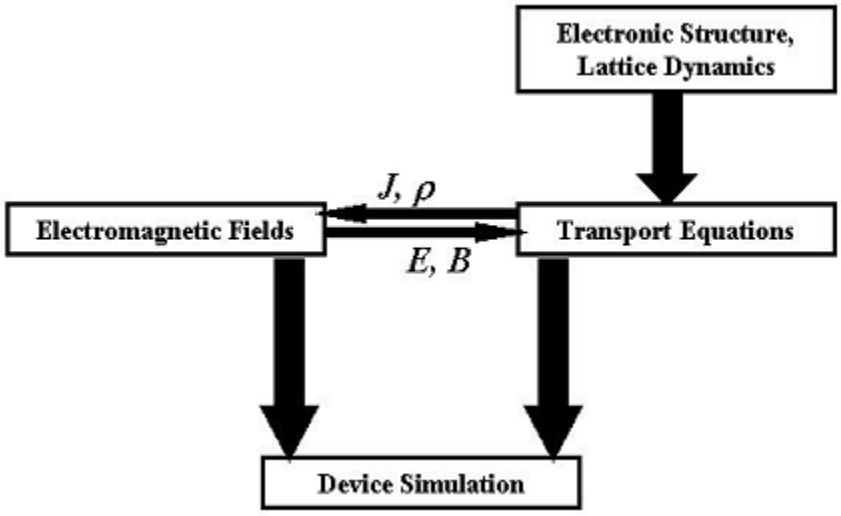

Figure 2.1 Schematic description of the device simulation sequence

(Courtesy of Dr. Vasileska& Dr. Goodnick)

2.2. SILVACO

Silvaco's ATLAS ™ is a versatile and modular program designed for two and three-dimensional device simulation. This device modeling and simulation software package by Silvaco International Corp. was used to perform the modeling in this thesis work. Silvaco's ATLAS™ program performed the device structuring and subprogram calls, while BLAZE™ and GIGA™ , ATLAS™ sub-modules (Figure 2.2), perform specialized functions required for advanced materials, heterojunctions, and thermal

modeling. To control, modify, and display the modeling and simulation, the Virtual Wafer Fabrication (VWF) Interactive Tools, namely DECKBUILD™ and TONYPLOT™ were utilized (see Figure 2.3 below).

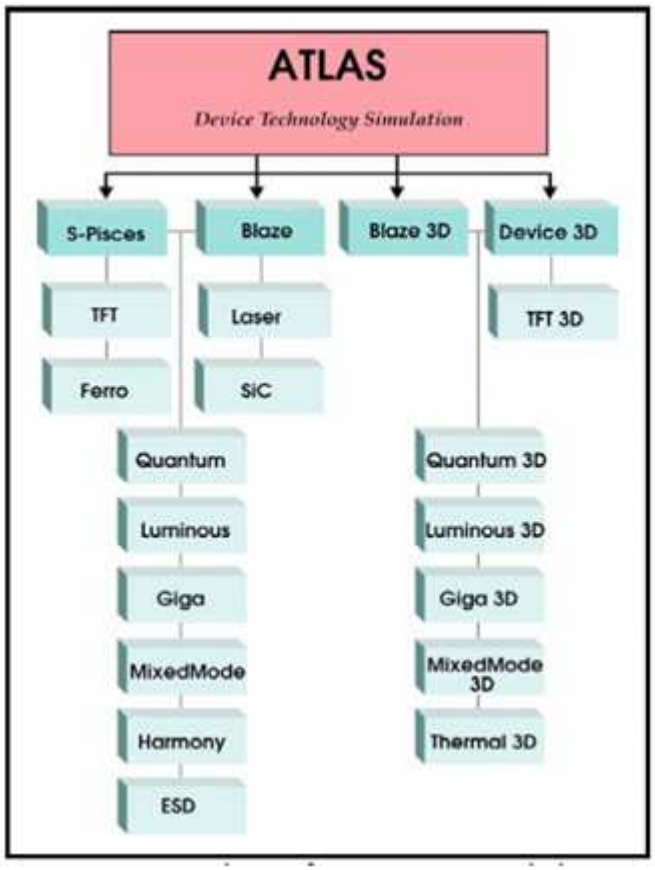

Figure 2.2 Representation of ATLAS' modular structure[30].

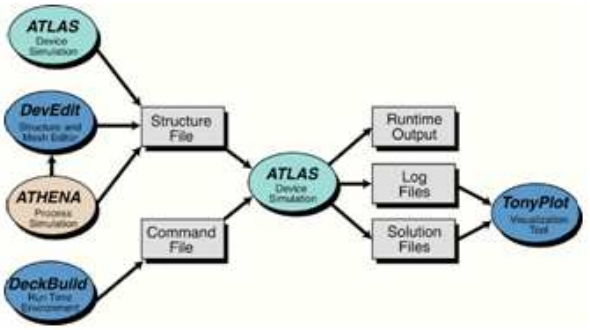

Figure 2.3 Flowchart of ATLAS' inputs and outputs[30]

Unlike some other modeling software, Silvaco uses physics-based simulation rather than empirical modeling. In truth, empirical modeling produces reliable formulas that will match existing data but physics-based simulation predicts device performance based upon physical structure and bias conditions. Silvaco software models a device in either two- or three-dimensional matrix-mesh format. Each mesh point represents a physical location within the modeled device and at that point, the program simulates transport properties via differential equations derived from Maxwell's equations. Numerical analysis is used to solve for electrostatic potential and carrier densities within the model. In addition to Poisson's equation, the continuity equations and the transport equations; the Lattice Heat Flow equation is added by using GIGA^{TM} .The heat generation term in the Lattice Heat Flow equation is further enhanced in this model by utilizing the Joule Heating function of GIGA ^{TM}.

To accurately model the III-V semiconductors, ATLAS must employ the BLAZE program extension to modify calculations that involve energy bands at heterojunctions .

The heterojunctions require changes in calculating current densities, thermionic emissions, velocity saturation, and recombination-generation.

ATLAS attempts to find solutions to carrier parameters such as current through electrodes, carrier concentrations, and electric fields throughout the device. ATLAS sets up the equations with an initial guess for parameter values then iterates through parameters to resolve discrepancies. ATLAS will alternatively use a decoupled (Gummel) approach or a coupled (Newton) approach to achieve an acceptable correspondence of values. When convergence on acceptable values does not occur, the program automatically reduces the iteration step size. ATLAS generates the initial guess for parameter values by solving a zero-bias condition based on doping profiles in the device.

2.3. Device Structures Being Simulated

This work focuses on two GaN HEMT structures. One is an $Al_{0.25}Ga_{0.75}N$/GaN HEMT. A GaN/AlGaN/AlN/GaN device is also being simulated. Inserting a very thin AlN interfacial layer between the AlGaN and GaN layers helps to increase the sheet charge density and improves mobility of the carriers in the channel. This owes to the reduction of alloy disorder scattering in AlGaN/AlN/GaN HEMT's when compared to AlGaN/GaN HEMT's. Since, the barrier height (conduction band difference) of AlN/GaN layer is larger than AlGaN/GaN layer, the probability of the channel electrons entering the AlGaN layer reduces significantly. This helps in reducing the impact of alloy

disorder scattering on the electron mobility, arising from the defects in the AlGaN layer[31-34].

2.3.1. AlGaN/GaN HEMT

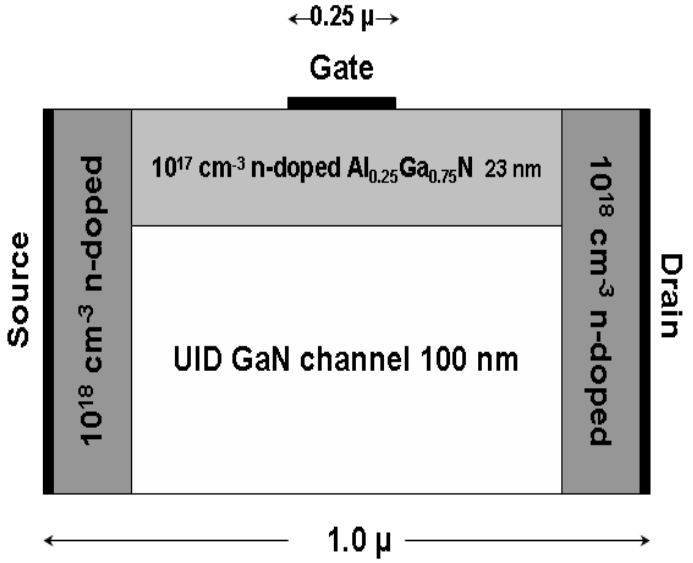

Figure 2.4 Simulated 2D AlGaN/GaN HEMT Structure.

Figure 2.4 shows the simulated AlGaN/GaN HEMT structure. A 23nm unintentionally doped AlGaN layer was formed on 100nm of the unintentionally doped GaN layer. An unintentionally doping of 10^{17} cm^{-3} is assumed for both the AlGaN and GaN layers. The source and drain electrodes are Ohmic contacts and are doped to 10^{18} cm^{-3}. The gate electrode is a Schottky contact, and the Schottky barrier height is calculated to be equal to 1.17eV[35].Figure 2.5 is the ATLAS-generated representation of the $Al_{0.25}Ga_{0.75}N$/GaNHEMT device.

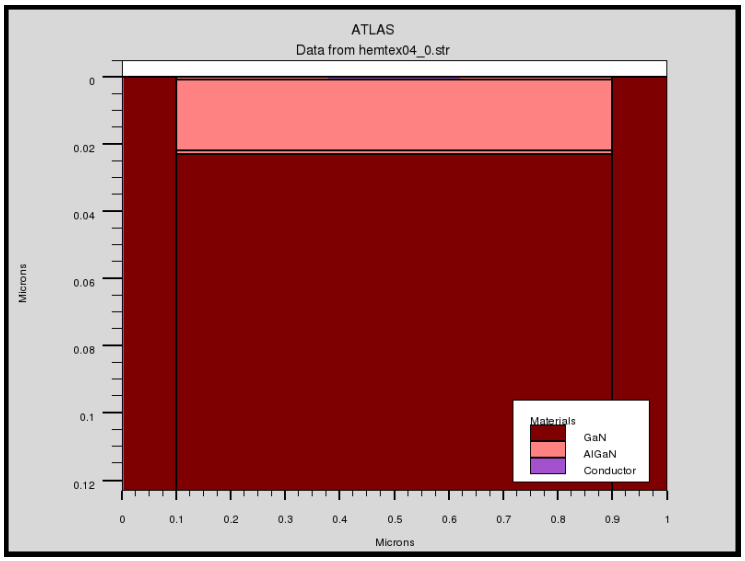

Figure 2.5 ATLAS generated representation of doped AlGaN/GaN HEMT.

2.3.2. GaN/AlGaN/AlN/GaN HEMT

Figure 2.6 shows the simulated GaN/AlGaN/AlN/GaN HEMT structure. It consists of a 1nm AlN layer grown on 100nm of GaN layer, a 16nm AlGaN layer on the top of AlN layer and a 3nm GaN cap layer. All the layers are unintentionally doped with a doping of $10^{16}cm^{-3}$.The source and drain are ohmic contacts and are doped to $10^{18}cm^{-3}$. The gate is a Schottky contact made of gold. Use of GaN cap layer has been found to be effective in confining electrons in the channel and minimize short channel effect.Figure 2.7 is the ATLAS-generated representation of the $Al_{0.28}Ga_{0.72}N$/AlN/GaNHEMT.

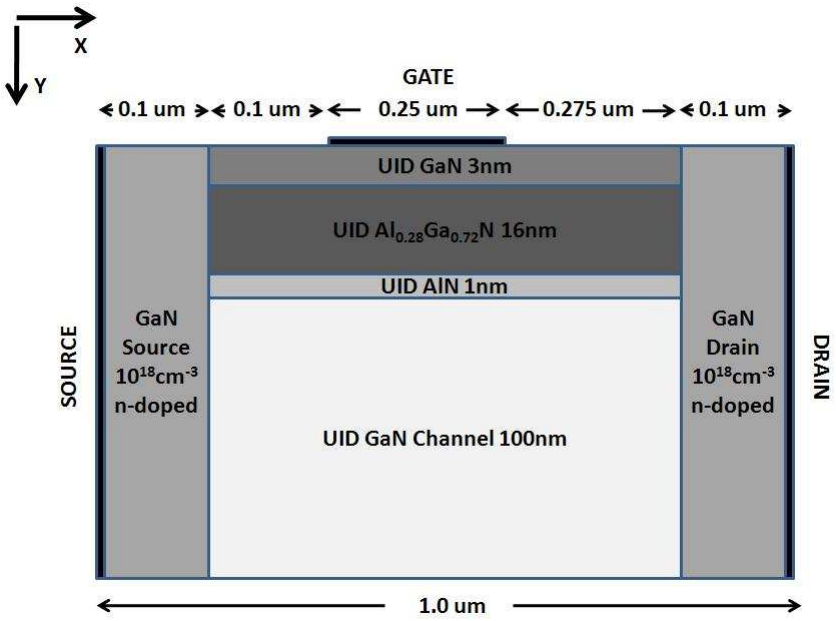

Figure 2.6 Simulated 2D GaN/AlGaN/AlN/GaN structure.

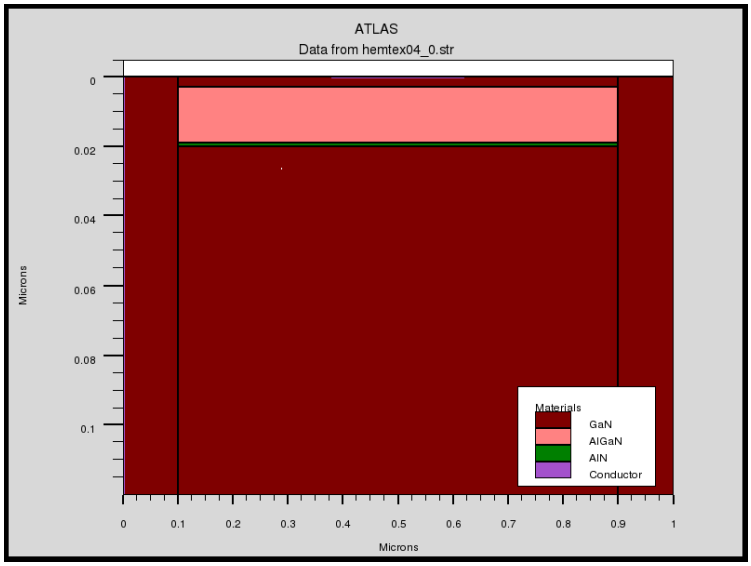

Figure 2.7 ATLAS generated representation of doped GaN/AlGaN/AlN/GaN HEMT.

2.4. Physical and Material Models

Silvaco ATLAS is used for the two-dimensional simulation of the GaN HEMT. To

accurately model the III-V semiconductors, ATLAS must employ the BLAZE program extension to modify calculations that involve energy bands at the heterostructure.

The heterojunctions require change in calculating current densities, velocity saturation and recombination-generation. The hydrodynamic/Energy Balance carrier transport model is used to achieve maximum accuracy as well as computational efficiency. This model takes account of non-local carrier heating effects for device structures with gate length less than 0.5 microns. As AlGaN/GaN HEMTs are unipolar devices, computational effort is reduced by neglecting the transport equations for holes in this work.

When using TCAD simulation software, a number of physical models have to be included into the model to perform simulations and do reliable predictions about device characteristics so that they closely match real device data. These models deal with the carrier behavior in combined effects of boundary conditions such as lattice temperature, electrostatic potential and fields, external forces and hetero-structures bandgap variations. Because of the high operating voltages, self-heating effects need to be accounted for in the model construction.

2.4.1. Drift-Diffusion(DD) Transport Model(Homogenous Structure)

Drift-diffusion is a transport model which approximates that the carrier flow inside the device is due to the drift and diffusion under an external lateral or longitudinal

field concurrently with recombination and generation processes. The current density is given by [36]:

$$J_n = -nq\mu_n \nabla \phi_n \tag{2.1}$$

$$J_p = -pq\mu_p \nabla \phi_p \tag{2.2}$$

Where μ_n and μ_p are electron and hole mobility respectively , ϕ_n and ϕ_p are the respective quasi Fermi levels ,*p* is the hole density and *n* is electron density. The quasi Fermi levels are linked to the carrier concentrations and the potential through the Boltzmann approximation:

$$n = n_{ie} \exp\left[\frac{q(\psi - \varphi_n)}{kT_L}\right] \tag{2.3}$$

$$p = n_{ie} \exp\left[\frac{q(\psi - \varphi_p)}{kT_L}\right] \tag{2.4}$$

Where n_{ie} is the effective intrinsic concentration and T_L is the lattice temperature ,*k* is the Boltzmann's constant, kT_L is the thermal energy in the system. These two equations may be rewritten to give the quasi-Fermi levels:

$$\varphi_n = \Psi - \frac{kT_L}{q} \ln \frac{n}{n_{ie}} \tag{2.5}$$

$$\varphi_p = \Psi - \frac{kT_L}{q} \ln \frac{p}{n_{ie}} \tag{2.6}$$

By substituting these equations into the current density equations, the following equations are obtained:

$$\overrightarrow{J_n} = qD_n \nabla n - qn\mu_n \nabla \psi - \mu_n n(kT_L \nabla(\ln n_{ie})) \quad (2.7)$$

$$\overrightarrow{J_p} = qD_p \nabla p - qp\mu_p \nabla \psi - \mu_p p(kT_L \nabla(\ln n_{ie})) \quad (2.8)$$

The final term accounts for the gradient in the effective intrinsic carrier concentration, which takes account of the bandgap narrowing effects. Effective electric fields are defined normally as:

$$\overrightarrow{E_n} = -\nabla(\psi + \frac{kT_L}{q} \ln n_{ie}) \quad (2.9)$$

$$\overrightarrow{E_p} = -\nabla(\psi + \frac{kT_L}{q} \ln n_{ie}) \quad (2.10)$$

Which then allows the more conventional formulation of drift-diffusion equations to be written:

$$\overrightarrow{J_n} = qn\mu_n \overrightarrow{E_n} + qD_n \nabla n \quad (2.11)$$

$$\overrightarrow{J_p} = qp\mu_p \overrightarrow{E_p} - qD_p \nabla p \quad (2.12)$$

This derivation has assumed that Einstein relationship holds. In case of Boltzmann statistics this corresponds to:

$$D_n = \frac{kT_L}{q} \mu_n \quad (2.13)$$

$$D_p = \frac{kT_L}{q} \mu_p \quad (2.14)$$

If Fermi-Dirac statistics are assumed for electrons then equation(2.13) becomes:

$$D_n = \frac{(\frac{kT_L}{q}\mu_n)F_{1/2}\left\{\frac{1}{kT_L}[\varepsilon_{Fn} - \varepsilon_C]\right\}}{F_{-1/2}\left\{\frac{1}{kT_L}[\varepsilon_{Fn} - \varepsilon_C]\right\}} \tag{2.15}$$

Where F_α is Fermi-Dirac integral of order α and ε_{Fn} is given by - $q\phi_n$.

2.4.2. Drift-diffusion with Position Dependent Band Structure(Heterostructure)

The current density equations must be modified to take into account the non-uniform band structure[37].The current density equations are [38]:

$$\overrightarrow{J_n} = -n\mu_n \nabla \phi_n \tag{2.16}$$

$$\overrightarrow{J_p} = -n\mu_p \nabla \phi_p \tag{2.17}$$

Where μ_n and μ_p are electron and hole mobility respectively, ϕ_n and ϕ_p are the respective quasi Fermi levels.

$$\phi_n = \frac{1}{q}E_{FN} \tag{2.18}$$

$$\phi_p = \frac{1}{q}E_{FP} \tag{2.19}$$

The conduction and valence band edge energies can be written as:

$$E_C = q(\psi_0 - \psi) - \chi \tag{2.20}$$

$$E_V = q(\psi_0 - \psi) - \chi - E_g \tag{2.21}$$

Where ψ_0 is some reference potential, χ is position dependent electron affinity, E_g is position dependent bandgap and

$$\psi_0 = \frac{\chi_r}{q} + \frac{kT_L}{q}\ln\frac{N_{cr}}{n_{ir}} = \frac{\chi_r + E_g}{q} - \frac{kT_L}{q}\ln\frac{N_{vr}}{n_{ir}} \tag{2.22}$$

wheren_{ir} is the intrinsic carrier concentration of the selected reference material, and *r* is the index that indicates that all of the parameters are taken from reference material. Fermi energies are expressed in the form:

$$E_{FN} = E_C + kT_L ln\frac{n}{N_c} - kT_L \ln \gamma n \tag{2.23}$$

$$E_{FP} = E_V + kT_L ln\frac{n}{N_v} - kT_L \ln \gamma n \tag{2.24}$$

The last terms on the RHS in equations (2.23) and(2.24)are due to the influence of Fermi-Dirac statistics. These final terms are defined as follows:

$$\gamma_n = \frac{F_{1/2}(\eta_n)}{e^{\eta_n}} \quad , \qquad \eta_n = \frac{E_{FN} - E_C}{kT_L} = F_{1/2}^{-1}\left(\frac{n}{N_c}\right) \tag{2.25}$$

$$\gamma_p = \frac{F_{1/2}(\eta_p)}{e^{\eta_p}} \quad , \quad \eta_p = \frac{E_v - E_{Fp}}{kT_L} = F_{1/2}^{-1}\left(\frac{p}{N_p}\right) \tag{2.26}$$

Where N_c and N_v are position dependent and $\gamma_n = \gamma_p = 1$ for Boltzmann statistics. By combining the above results, one can obtain the following expression for the current densities:

$$\overrightarrow{J_n} = kT_L\mu_n\nabla n - q\mu_n\nabla n\left(\psi + \frac{kT_L}{q}\ln\gamma_n + \frac{\chi}{q} + \frac{kT_L}{q}\ln\frac{N_C}{n_{ir}}\right) \quad (2.27)$$

$$\overrightarrow{J_p} = kT_L\mu_p\nabla p - q\mu_p\nabla p\left(\psi + \frac{kT_L}{q}\ln\gamma_p + \frac{\chi + E_g}{q} + \frac{kT_L}{q}\ln\frac{N_V}{n_{ir}}\right) \quad (2.28)$$

2.4.3. Hydrodynamic/Energy Balance Transport Model

The conventional drift-diffusion model of charge transport neglects non–local transport effects such as velocity overshoot, diffusion associated with the carrier temperature and the dependence of impact ionization rates on carrier energy distributions. These phenomena can have a significant effect in case of submicron devices. As a result ATLAS offers two non-local models of charge transport, the energy balance and the hydrodynamic models. The Energy Balance Transport Model follows the derivation by Stratton [39,40]. Hydrodynamic model is derived from this model by applying certain assumptions[41,42,43].

The Energy Balance Transport Model adds continuity equations for the carrier temperatures, and treats mobilities and impact ionization coefficients as functions of the carrier temperatures(T_n,T_p) rather than functions of the local electric field. For electrons, the Energy Balance Transport Model consists of:

$$div\overrightarrow{S_n} = \frac{1}{q}\overrightarrow{J_n}.\overrightarrow{E} - W_n - \frac{3k}{2}\frac{\partial}{\partial t}(\lambda_n^* nT_n) \quad (2.29)$$

$$\overrightarrow{J_n} = qD_n\nabla n - qn\mu_n\nabla\psi + qnD_n^T\nabla T_n \quad (2.30)$$

$$\overrightarrow{S_n} = -K_n \nabla T_n - \left(\frac{k\delta_n}{q} \right) \overrightarrow{J_n} T_n \tag{2.31}$$

$$W_n = \frac{3}{2} n \frac{k\left(T_n - T_L\right)}{TAUREL.EL} \lambda_n + \frac{3}{2} k T_n \lambda_n R_{SRH} + E_g \left(G_n - R_n{}^A\right) \tag{2.32}$$

$$\lambda_n = F_{\frac{3}{2}}(h_n) / F_{\frac{1}{2}}(h_n) \tag{2.33}$$

And for holes:

$$div\overrightarrow{S_p} = \frac{1}{q} \overrightarrow{J_p} . \vec{E} - W_p - \frac{3k}{2} \frac{\partial}{\partial t} (\lambda_p{}^* n T_p) \tag{2.34}$$

$$\overrightarrow{J_p} = -qD_p \nabla p - qp\mu_p \nabla \psi + qpD_p{}^T \nabla T_p \tag{2.35}$$

$$\overrightarrow{S_p} = -K_p \nabla T_p - \left(\frac{k\delta_p}{q} \right) \overrightarrow{J_p} T_p \tag{2.36}$$

$$W_p = \frac{3}{2} p \frac{k\left(T_p - T_L\right)}{TAUREL.HO} \lambda_p + \frac{3}{2} k T_p \lambda_p R_{SRH} + E_g \left(G_p - R_p{}^A\right) \tag{2.37}$$

$$\lambda_p = F_{\frac{3}{2}}(h_p) / F_{\frac{1}{2}}(h_p) \tag{2.38}$$

Where $\overrightarrow{S_n}$ and $\overrightarrow{S_p}$ are energy flux densities associated with electrons and holes, and μ_n and μ_p are the electron and hole mobilities, R_{SRH} is the SRH recombination rate, $R_n{}^A$ and $R_p{}^A$ are Auger recombination rates related to electron and holes, G_n and G_p are impact ionization rates, TAUREL.EL and TAUREL.HO are the electron and hole energy relaxation times, E_g is the banggap energy of the semiconductor. The relaxation parameters are user-definable on the MATERIAL statement. The relaxation times are

extremely important as they define the time constant for the rate of energy exchange and therefore accurate values are required if the model is to be accurate.

The remaining terms, D_n and D_p are the thermal diffusivities for electrons and holes. W_n and W_p are the energy density loss rates for electrons and holes as defined in (2.32) and (2.37) respectively. Thus, the following relationships hold:

$$D_n = \frac{\mu_n k T_n}{q} \lambda_n^* \tag{2.39}$$

$$\lambda_n^* = \frac{F(1/2)(\eta_n)}{F(-1/2)(\eta_n)} \tag{2.40}$$

$$\text{where } \eta_n = \frac{\varepsilon_{F_n} - \varepsilon_C}{kT_n} = F_{1/2}{}^{-1}\left(\frac{n}{N_C}\right) \tag{2.41}$$

$$D_n^T = (\mu_{2n} - \frac{3}{2}\lambda_n^* \mu_n)\frac{k}{q} \tag{2.42}$$

$$\mu_{2n} = \mu_n\left(\frac{5}{2} + \xi_n\right)\frac{F_{\xi n} + 3/2(\eta_n)}{F_{\xi n} + 1/2(\eta_n)} \tag{2.43}$$

$$Kn = q.n\mu_n\left(\frac{k}{q}\right)^2 \Delta_n T_n \tag{2.44}$$

$$\Delta_n = \delta_n\left[\left(\xi_n + \frac{7}{2}\right)\frac{F_{\xi n} + 5/2(\eta_n)}{F_{\xi n} + 3/2(\eta_n)} - \left(\xi_n + \frac{5}{2}\right)\frac{F_{\xi n} + 3/2(\eta_n)}{F_{\xi n} + 1/2(\eta_n)}\right] \tag{2.45}$$

$$\delta_n = \frac{\mu_{2n}}{\mu_n} \tag{2.46}$$

Similar expressions for holes are as follows:

$$D_p = \frac{\mu_p k T_p}{q} \lambda_p^* \tag{2.47}$$

$$\lambda_p^* = \frac{F(1/2)(\eta_p)}{F(-1/2)(\eta_p)} \tag{2.48}$$

where
$$\eta_p = \frac{\varepsilon_V - \varepsilon_{f_p}}{kT_p} = F_{1/2}^{-1}(\frac{p}{N_V}) \tag{2.49}$$

$$D_p^T = (\mu_{2p} - \frac{3}{2}\lambda_p^* \mu_p)\frac{k}{q} \tag{2.50}$$

$$\mu_{2p} = \mu_p(\frac{5}{2} + \xi_p)\frac{F_{\xi p} + 3/2(\eta_p)}{F_{\xi p} + 1/2(\eta_p)} \tag{2.51}$$

$$Kp = q.p\mu_p(\frac{k}{q})^2 \Delta_p T_p \tag{2.52}$$

$$\Delta_p = \delta_p \left[\left(\xi_p + \frac{7}{2} \right) \frac{F_{\xi p} + 5/2(\eta_p)}{F_{\xi p} + 3/2(\eta_p)} - \left(\xi_p + \frac{5}{2} \right) \frac{F_{\xi p} + 3/2(\eta_p)}{F_{\xi p} + 1/2(\eta_p)} \right] \tag{2.53}$$

$$\delta_p = \frac{\mu_{2p}}{\mu_p} \tag{2.54}$$

K_n and K_p are thermal conductivities of electrons and holes as defined in (2.44) and (2.52) respectively. If Boltzmann statistics are used in preference to Fermi statistics, the above equations simplify to :

$$\lambda_n^* = \lambda_p^* = 1 \tag{2.55}$$

$$\Delta_n = \delta_n = \left[\frac{5}{2} + \xi_n\right] \tag{2.56}$$

$$\Delta_p = \delta_p = \left[\frac{5}{2} + \xi_p\right] \tag{2.57}$$

$$\xi_n = \frac{d(\ln \mu_n)}{d(\ln T_n)} = \frac{T_n}{\mu_n}\frac{\partial \mu_n}{\partial T_n} \tag{2.58}$$

$$\xi_p = \frac{d(\ln \mu_p)}{d(\ln T_p)} = \frac{T_P}{\mu_P}\frac{\partial \mu_P}{\partial T_P} \tag{2.59}$$

The parameters ξ_n and ξ_p are carrier temperature dependent. Different assumptions regarding ξ_n and ξ_p correspond to different non-local models. In the high-field saturated velocity model , the carrier mobilities are inversely proportional to carrier temperature. Thus:

$$\xi_n = \xi_p = -1 \tag{2.60}$$

corresponds to Energy Balance Transport Model. Furthermore when

$$\xi_n = \xi_p = 0\,, \tag{2.61}$$

this corresponds to the simplified Hydrodynamic Transport Model.

The parameters ξ_n and ξ_p can be specified using the KSN and KSP parameters in the MODELS statement.

Hot carrier transport equations are activated by the MODELS statement parameter: HCTE.EL (electron temperature),HCTE.HL(hole temperature),HCTE(both carrier temperature)[38].

2.4.4. Hydrodynamic Boundary conditions

Boundary conditions for *n,p* and ψ are same as for drift-diffusion model. Energy balance equations are solved only in the semiconductor region. Electron and hole temperatures are set equal to lattice temperature on the contacts. On the other part of the boundary , the normal components of the energy fluxes vanish.

2.4.5. Boundary Physics: Ohmic and Schottky Contact

Many of useful properties of p-n junctions can be achieved by forming different metal-semiconductor contacts[44].The major difference between ohmic and Schottky contact is the Schottky barrier height, ϕ_B, is non-positive or positive. For ohmic contacts, the barrier height should be near zero or negative, formed accumulation type contact, thus the majority carriers are free to flow out the semiconductors, as shown below in Figure 2.8. On the contrary, for Schottky contacts, the barrier height would be positive, built depletion type contacts, so that the majority carriers cannot be absorbed freely due to the band bending caused by positive barrier height. Hence the way they are implemented in the simulator is different.

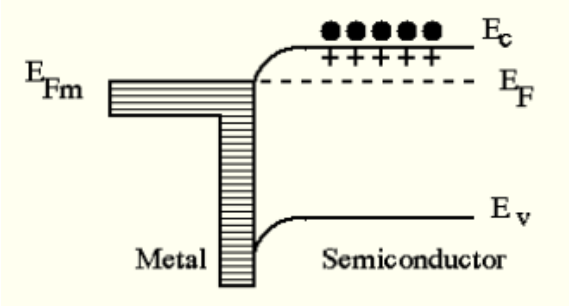

Figure 2.8 Accumulation type ohmic contact.

2.4.5.1. Ohmic Contacts

Ohmic contacts are implemented as simple Dirichlet's boundary condition, where surface potential, hole concentration and electron concentration are fixed (Ψ_s, n_s, p_s). Minority and majority carrier quasi-Fermi potentials are equal to the applied bias of the electrode $(\phi_n = \phi_p = V_{applied})$. The potential ψ_s is fixed at a value that is consistent with space charge neutrality. If Boltzmann statistics is used then

$$\psi_s = \phi_n + \frac{kT_L}{q}\ln\frac{n_s}{n_{ie}} = \phi_p - \frac{kT_L}{q}\ln\frac{p_s}{n_{ie}} \qquad (2.62)$$

where n_{ie} is intrinsic carrier concentration[38].

If work function is not specified, the contact will be ohmic regardless of the material.

2.4.5.2. Schottky Contacts

The surface potential of the Schottky contact is given by:

$$\psi_s = AFFINITY + \frac{E_g}{2q} + \frac{kT_L}{2q}\ln\frac{N_C}{N_V} - WORKFUN + V_{applied} \qquad (2.63)$$

where AFFINITY is the electron affinity of the semiconductor material, E_g is the bandgap,N_c is the conduction band density of states, N_v is the valence band density of states, and T_L is the ambient temperature. The workfunction is defined as:

WORKFUN=AFFINITY+ ϕ_B (2.64)

Where ϕ_B is the barrier height at the metal-semiconductor interface in eV[38].A Schottky contact[45]is implemented by specifying workfunction using the WORKFUN in the parameter of the contact statement.

2.4.6. Mobility Model

There are two types of electric field dependent mobility models used in ATLAS/BLAZE. These models are Standard Mobility Model and Negative Differential Mobility Model. The standard mobility model takes account of velocity saturation. The following Caughey and Thomas expression[46] is used to implement a field-dependent mobility:

$$\mu_n(E) = \mu_{n0}\left[\frac{1}{1+\left(\frac{\mu_{n0}E}{VSATN}\right)^{BETAN}}\right]^{\frac{1}{BETAN}} \qquad (2.65)$$

$$\mu_p(E) = \mu_{p0}\left[\frac{1}{1+\left(\frac{\mu_{p0}E}{VSATP}\right)^{BETAP}}\right]^{\frac{1}{BETAP}} \qquad (2.66)$$

Here, E is the parallel electric field and μ_{n0} and μ_{p0} are low field electron and hole mobilities respectively. VSATN and VSATP are saturation velocities for electrons and holes respectively. The low field mobilities are calculated by one of the low-field mobility models. BETAN and BETAP parameters have default values(see Table 2.1). The VSATN, VSATP, BETAN and BETAP parameters are user definable in the material statement. This model is activated by specifying EVSATMOD=0 and FLDMOB in the MODEL statement. It is this model that has been used in the simulation of the HEMT structures shown in Section 2.3 .

The Negative Differential Mobility Model is activated by specifying EVSATMOD=1 and FLDMOB in the MODEL statement. It is a temperature dependent mobility model.It introduces an instability in the solution process. It is used for devices where the drift velocity peaks at some electric field before reducing with increase in the electric field[45].

The Hydrodynamic Transport Model requires the carrier mobility to be related to carrier energy. An effective electric field is calculated, which causes the carriers to attain the same temperature as at the node point in the device. The effective electric fields, $E_{eff,n}$ and $E_{eff,p}$ are then calculated by solving the equations:

$$q\mu_n\left(E_{eff,n}\right)E^2{}_{eff,n} = \frac{3}{2}\frac{k(T_n - T_L)}{TAUMOB.EL} \tag{2.67}$$

$$q\mu_P\left(E_{eff,n}\right)E^2{}_{eff,p} = \frac{3}{2}\frac{k(T_p - T_L)}{TAUMOB.HO} \tag{2.68}$$

These equations are derived from energy balance equations by stripping out all the spatially varying terms. The effective electric fields are then introduced into the relevant field dependent mobility model.

The resultant relationship between carrier mobility and carrier temperature is given by:

$$\mu_n = \frac{\mu_{n0}}{\left(1 + X_n^{BETAN}\right)^{\frac{1}{BETAN}}} \tag{2.69}$$

$$\mu_P = \frac{\mu_{P0}}{\left(1 + X_P^{BETAP}\right)^{\frac{1}{BETAP}}} \tag{2.70}$$

$$X_n^{BETAN} = \frac{1}{2}\left(\alpha_n^{BETAN}(T_n - T_L)^{BETAN} + \sqrt{\alpha_n^{2BETAN}(T_n - T_L)^{2BETAN} - 4\alpha_n^{BETAN}(T_n - T_L)^{BETAN}}\right) \tag{2.71}$$

$$X_P^{BETAN} = \frac{1}{2}\left(\alpha_P^{BETAP}(T_P - T_L)^{BETAP} + \sqrt{\alpha_P^{2BETAP}(T_P - T_L)^{2BETAP} - 4\alpha_P^{BETAP}(T_P - T_L)^{BETAP}}\right) \tag{2.72}$$

$$\alpha_n = \frac{3}{2}\frac{k_B\mu_{n0}}{qVSATN^2\left(TAUREL.EL\right)} \tag{2.73}$$

$$\alpha_p = \frac{3}{2}\frac{k_B\mu_{p0}}{qVSATP^2\left(TAUREL.HO\right)} \tag{2.74}$$

As carriers are accelerated in an electric field, their velocity will begin to saturate when the electric field magnitude becomes significant. This effect has to be accounted for by a reduction of effective mobility since the magnitude of drift velocity is the product of mobility and the electric field component in the direction of the current flow. This provides a smooth transition between low-field and high field behavior.

The saturation velocities are calculated by default from the temperature dependent model[47]:

$$VSATN = \frac{ALPHAN.FLD}{1 + THETAN.FLD \exp\left(\frac{T_L}{TNOMN.FLD}\right)} \tag{2.75}$$

$$VSATP = \frac{ALPHAP.FLD}{1 + THETAP.FLD \exp\left(\frac{T_L}{TNOMP.FLD}\right)} \tag{2.76}$$

One can set them to constant values on the MOBILITY statement using VSATN and VSATP parameters.

Table 2.1 User definable parameters in field-dependent mobility model.

Statement	Parameter	Default	Units
MOBILITY	ALPHAN.FLD	$2.4X10^7$	cm/s
MOBILITY	ALPHAP.FLD	$2.4X10^7$	cm/s
MOBILITY	BETAN	2.0	
MOBILITY	BETAP	1.0	
MOBILITY	THETAN.FLD	0.8	
MOBILITY	THETAP.FLD	0.8	
MOBILITY	TNOMN.FLD	600.0	K
MOBILITY	TNOMP.FLD	600.0	K

2.4.7 Spontaneous and Piezoelectric Polarization Implementation

A good understanding of the electrical polarization effects at the $Al_xGa_{1-x}N/GaN$ interface is a key to proper device simulation. The spontaneous polarization P_{sp} and the strain induced piezoelectric polarization P_z are calculated by using:

$$P_{sp} = P_{sp}Al_xGa_{1-x}N + P_{sp}\,GaN\,(1-x) \tag{2.77}$$

$$P_z = 2\frac{a_s - a_0}{a_0}\left(e_{31} - e_{33}\frac{c_{13}}{c_{33}}\right) \tag{2.78}$$

where a_0 and a_s are lattice constants and e_{31} and e_{33} are piezoelectric coefficients and c_{13}, c_{33} are elastic constants[36].In this simulation, this interface charge was implemented by making the region near the heterojunction highly doped n-type at the interface.

2.5. Self-heating Simulations

This section briefly describes the models used to simulate self-heating effects with TCAD. These models are described in more details in the simulator manual[38]. Briefly, the non-isothermal model modifies the drift-diffusion equations to account for the self-heating effects. The assumption here is that the lattice is in thermal equilibrium with the charge carriers. This implies that carrier and lattice temperature are described by a single quantity T_L. T_L is calculated by coupling the lattice heat equation and the modified drift-diffusion equation.

2.5.1. Overview

GIGA module extends the Silvaco TCAD software to account for lattice heat flow and general thermal environments. GIGA implements Wachutka's thermodynamically rigorous model of lattice heating[48], which account for Joule heating, heating and cooling due to carrier generation and recombination , and Peltier and Thomson effects.

2.5.2 Numerics

GIGA module supplies numerical techniques that provide efficient solution of equations that result when lattice heating is accounted for. These numerical techniques include fully-coupled and block iteration method. When GIGA is used with energy balance equations, the result is a solver for six PDEs.

2.5.3 Non-Isothermal Models

2.5.3.1 The Lattice Heat Flow Equation

GIGA adds the heat flow equation to the primary equations that are solved by ATLAS. The heat flow equation has the form:

$$C\frac{\partial T_L}{\partial t} = \nabla\left(\kappa \nabla T_L\right) + H \qquad (2.79)$$

where:

C is the heat capacitance per unit volume

κ is the thermal conductivity

H is the heat generation

T_L is the local lattice temperature

The heat capacitance can be expressed as $C = \rho C_P$, where C_P is the specific heat and ρ is the density of the material. Specifying the LAT.TEMP parameter in the MODEL statement includes the lattice heat flow equations in the ATLAS simulations.

GIGA supports different combinations of models. If the HCTE and LAT.TEMP parameters are specified in the MODELS statement and both particle continuity

equations are solved, all six equations are solved. If HCTE.EL is specified instead of HCTE, only five equations are solved and hole temperature T_p is set equal to lattice temperature T_L.

2.5.3.2 Effective Density of States

When lattice heating is specified with energy balance model, the effective densities of states are modeled as functions of the local carrier temperature , T_n and $T_{p,}$ as defined by:

$$N_C = \left(\frac{2\pi m_e^* kT_n}{h^2} \right)^{\frac{3}{2}} = \left(\frac{T_n}{300} \right)^{\frac{3}{2}} NC(300) \qquad (2.80)$$

$$N_V = \left(\frac{2\pi m_P^* kT_p}{h^2} \right)^{\frac{3}{2}} = \left(\frac{T_p}{300} \right)^{\frac{3}{2}} NV(300) \qquad (2.81)$$

2.5.3.3 Non-Isothermal Current Densities

When GIGA is used, the electron and hole current densities are modified to account for lattice temperatures:

$$\overrightarrow{J_n} = -q\mu_n n(\nabla\phi_n + P_n \nabla T_L) \qquad (2.82)$$

$$\overrightarrow{J_p} = -q\mu_p p(\nabla\phi_p + P_p \nabla T_L) \qquad (2.83)$$

Where P_n and P_p are absolute thermoelectric powers for electrons and holes. P_n and P_p are expressed as follows:

$$P_n = -\frac{k_B}{Q}\left(\frac{5}{2} + \ln\frac{N_C}{n} + KSN + \xi_n\right) \tag{2.84}$$

$$P_p = \frac{k_B}{Q}\left(\frac{5}{2} + \ln\frac{N_V}{p} + KSP + \xi_p\right) \tag{2.85}$$

Here, k_B is the Boltzmann constant. KSN and KSP are the exponents in the power law relationship between relaxation time(mobility) and carrier energy. They are set on the MODELS statement. The quantities ξ_n and ξ_P are the phonon drag contribution to the thermopower. ATLAS has a built in model for it and specifying PHONONDRAG parameter on the MODELS statement enables it. The built-in model is:

$$\xi_n = \left(\frac{k_B}{Q}\right) PDA.N \left(\frac{T_L}{300}\right)^{PDEXP.N} \quad \text{for electrons} \tag{2.86}$$

$$\xi_p = \left(\frac{k_B}{Q}\right) PDA.P \left(\frac{T_L}{300}\right)^{PDEXP.P} \quad \text{for holes} \tag{2.87}$$

A theoretically derived value for PDEXP.N and PDEXP.N is $-7/2$ [49] but experimentally obtained value is close to $-5/2$ [50].The values of PDA.N and PDA.P depend on the doping level and sample size. So, one has to determine values to fit his sample.

The thermopower consists of three components. The first is the derivative of the Fermi Potential with respect to temperature. ATLAS incorporates this effect indirectly through the boundary conditions. For Maxwell-Boltzmann statistics, this is

$$-\frac{k_B}{Q}\left(\frac{3}{2}+\ln\frac{N_C}{n}\right)\text{for}\quad\text{electrons} \tag{2.88}$$

$$\frac{k_B}{Q}\left(\frac{3}{2}+\ln\frac{N_V}{p}\right)\text{for hole} \tag{2.89}$$

The second term is due to carrier scattering.

$$\frac{k_B}{Q}(1+KSN)\,\text{for electrons} \tag{2.90}$$

$$\frac{k_B}{Q}(1+KSP)\,\text{for holes} \tag{2.91}$$

The third term is the phonon drag contribution $-\xi_n$ and ξ_p. The second and third terms are included directly into the temperature gradient term in the expressions for current[38].

2.5.3.4. Heat generation

When carrier transport is handled in the drift-diffusion approximation the heat generation term H has the form:

$$\begin{aligned} H &= \frac{\left|\overrightarrow{J_n}\right|^2}{q\mu_n n}+\frac{\left|\overrightarrow{J_p}\right|^2}{q\mu_p p}-T_L\left(\overrightarrow{J_n}\nabla P_n\right)-T_L\left(\overrightarrow{J_p}\nabla P_p\right)\\ &+q(R-G)\left[T_L\left(\frac{\partial\phi_n}{\partial T}_{n,p}\right)-\phi_n-T_L\left(\frac{\partial\phi_p}{\partial T}_{n,p}\right)+\phi_p\right]\\ &-T_L\left(\frac{\partial\phi_n}{\partial T}_{n,p}+P_n\right)divJ_n-T_L\left(\frac{\partial\phi_p}{\partial T}_{n,p}+P_p\right)divJ_p \end{aligned} \tag{2.92}$$

In the steady-state case current divergence can be replaced with the net recombination, then the above equation simplifies to:

$$H = \left[\frac{\left|\overrightarrow{J_n}\right|^2}{q\mu_n n} + \frac{\left|\overrightarrow{J_p}\right|^2}{q\mu_p p} \right] + q(R-G)\left[\phi_p - \phi_n + T_L\left(P_p - P_n\right)\right] - T_L\left(\overrightarrow{J_n}\nabla P_n + \overrightarrow{J_p}\nabla P_p\right) \tag{2.93}$$

where:

$\left[\frac{\left|\overrightarrow{J_n}\right|^2}{q\mu_n n} + \frac{\left|\overrightarrow{J_p}\right|^2}{q\mu_p p} \right]$ is the Joule heating term , $q(R-G)\left[\phi_p - \phi_n + T_L\left(P_p - P_n\right)\right]$ is the recombination and generation heating and cooling term, $-T_L\left(\overrightarrow{J_n}\nabla P_n + \overrightarrow{J_p}\nabla P_p\right)$ accounts for the Peltier and Joule-Thomson effects . A simple form of H that is widely used is:

$$H = \left(\overrightarrow{J_n} + \overrightarrow{J_p}\right)\overrightarrow{E} \tag{2.94}$$

GIGA can use either equation(2.93) or (2.94) for steady-state calculations. By default, equation(2.94) is used. If HEAT.FULL in specified in the MODELS statement then equation(2.93) is used. To enable/disable individual terms of equation(2.93) one need to use JOULE.HEAT,GR.HEAT and PT.HEAT parameters on the MODEL statement. If the general expression shown in equation(2.92) is used for the non-stationary case, the derivatives $\left(\frac{\partial \phi_n}{\partial T}\right)_{n,p}$ and $\left(\frac{\partial \phi_p}{\partial T}\right)_{n,p}$ are evaluated for the case of an idealized non-degenerate semiconductor and complete ionization.

The heat generation term ,H is always set to 0 in insulators.

For conductors, $H = \frac{\left(\nabla V\right)^2}{\rho}$. (2.95)

When electron and hole transport are modeled in the energy balance approximation(by specifying HCTE on the MODELS statement)the following expression for H is used:

$H=W_n+W_p+E_gU$, (2.96)

where,

U is the net generation-recombination rate given by:

$$U = R_{srh} + R_n^{\ A} + R_P^{\ A} - G_n - G_p \quad (2.97)$$

R_{SRH} is the SRH recombination rate, $R_n^{\ A}$ and $R_p^{\ A}$ Auger recombination rates related to electron and holes, G_n and G_p are impact ionization rates.

If the energy balance model is enabled for only electrons or only for holes, then a hybrid of equations (2.96) and (2.93) or (2.94) is used. If the energy balance equation is solved for electrons, but not for holes, then H is evaluated as follows if HEAT.FULL is specified:

$$H = W_n + E_gU + \frac{\left|\overrightarrow{J_p}\right|^2}{q\mu_p p} - T_L\left(\overrightarrow{J_p}\nabla P_p\right) \quad (2.98)$$

A simpler form of heating will be used if HEAT.FULL is not specified.

$$H = W_n + E_gU + \overrightarrow{J_p}\overrightarrow{E} \quad (2.99)$$

The first terms of W_n and W_p are output to structure files as Joule heating. The last term(equation(2.98)) is output as Peltier Thomson heat power. The remaining terms are output as recombination heat power[38].

2.5.3.5. Thermal Boundary Condition

At least one thermal boundary condition must be specified when lattice flow equation is solved. The thermal boundary conditions used have the following general equation:

$$\sigma(\bar{J^u}_{tot}.\vec{s}) = \alpha(T_L - T_{ext}) \tag{2.100}$$

where σ is either 0 or 1, $\vec{J^u}_{tot}$ is the total energy flux, and $\vec{s}$ is the unit external normal of the boundary. The projection of the energy flux onto s is given by the equation:

$$\vec{J^u}_{tot}.\vec{s} = -\kappa\frac{\partial T_L}{\partial n} + (T_L P_n + \phi_n)\overrightarrow{J_n}.\vec{s} + (T_L P_p + \phi_p)\overrightarrow{J_p}.\vec{s} \tag{2.101}$$

When σ=0 , equation(2.100) specifies a Dirichlet (fixed temperature) boundary condition. One can specify Dirichlet boundary conditions for an external boundary or for an electrode inside the device. When σ=1 , equation(2.100) takes the form:

$$(\vec{J^u}_{tot}.\vec{s}) = \frac{1}{R_{th}}(T_L - TEMPER) \tag{2.102}$$

Where the thermal resistance, R_{th} is given by,

$$R_{th} = \frac{1}{ALPHA} \tag{2.103}$$

APLHA is user definable in THERMCONTACT statement.

Setting thermal boundary is similar to setting electrical boundary conditions. The THERMCONTACT statement is used to specify the position of the thermal contact. One

can place thermal contact anywhere in the device. When a value of alpha is used, equation (2.102) is used[38].

2.6 Gummel's Iteration Method for the Case of Drift-Diffusion Model

Gummel's method solves the coupled set of carriers' continuity equations together with the Poisson's Equation via a decoupled procedure. The potential profile obtained from equilibrium simulations is substituted into the continuity equations to obtain carrier's distribution profile. The result is then sent back into Poisson's Equation to calculate new electrostatic energy profiles. This process is repeated until convergence requirement is achieved, as shown in Figure. 2.9.

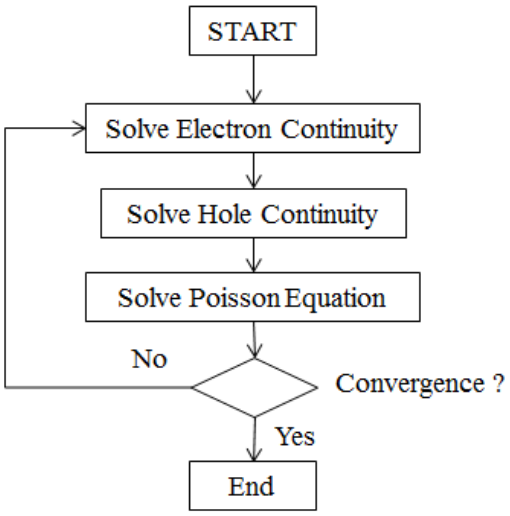

Figure 2.9 Gummel's iteration scheme

When hydrodynamic model is used, a for the isothermal case a set of 5 differential equations is solved in a sequential order. When self-heating are incorporated in the model,

an additional (6^{th}) PDE is solved to model the lattice temperature variation.

2.7. Model Development

Several assumptions were made when creating the model. One assumption is the gate, drain and source contacts in the model are treated as perfect electrical conductors. The interfaces between the layers were considered ideal with no modeled defects or surface modifications besides the interface charge to simulate the piezoelectric effect.

First it was attempted to create an electrically accurate 2-dimensional model of the device using 'polarization' function. After several unsuccessful attempts by this researcher using the 'polarization' function to accurately model the electrical effects of a hetero-junction, an interface charge was inserted at the AlGaN/GaN boundary using 'interface' function. That also did not work. Then the interface charge was implemented by using n doped AlGaN layer. When combined with a thin GaN region of increased mobility directly below the AlGaN/GaN junction, the desired effect is achieved. One of the goals of this research was to model the device in 2-dimensions.

Structuring the model to match the dimensional characteristics of the physical device was of paramount importance. Such an approach seemed the most logical with the end goal to eventually use 2-dimensional thermal modeling. The individual values that were most often modified throughout the model development were AlGaN layer thickness, Gate Work Function (WF), donor levels in AlGaN and GaN layers, the interface charge at the

heterojunction, momentum and energy relaxation rates, the electron mobilities and saturation velocities in each of the AlGaN and GaN layers. Final values were chosen through trial and error until the most accurate representation of IV curves was achieved.

Early on in the model development process, the donor levels(concentrations) were given the most attention. So a variety of layer concentration were modeled to determine which would give the closest electrical output characteristics to experimental results. AlGaN thickness did not have a notably strong effect on modeled device performance. Gate WF had the largest effect on device linearity and drain current over the modeled bias ranges. A gate WF of 4.73 eV is used to coincide with the generally accepted WF of a gate contact for a FET. Generally accepted ranges of available extra electrons at the heterojunction for the piezoelectric and polarization effects of a GaN HEMT are around 10^{13} cm^{-2}. Therefore, an interface charge near that level was necessary to model the piezoelectric effect. The 2-dimensional model closely resembled the electrical characteristics of the experimented device. The gate length in the model is 0.25 microns between 0.375 to 0.625 microns. Upper thin layer of GaN acts as channel and lower GaN layer works as substrate.

In this thesis, the Low Field Mobility Model chosen to simulate the device operation is Parallel Electric Field Dependent Mobility model. The same structure and same model was used throughout in the simulation. The effects of applying various parameters of Albrecht's model and the comparison with high field mobility models have been further discussed in the ATLAS manual.

Through model development several notable discoveries were made based on intermediate simulation results. GaN layer has most effect on the electrical characteristic of the device. During thermal simulation using small value of alpha prevents the model engine from converging and displays much higher maximum channel temperatures while the simulation is running when compared to a model that will converge with appropriate alpha value. Another discovery was that the upper GaN model layer representing channel would be as thin as 0.002 microns and the electrical results were identical over the same bias conditions reported by experiment. Thermal results were also identical over the same bias conditions when compared to the experimental model. Conditions at higher bias were not modeled during this research. One can postulate that decreasing the GaN layer will have multiple effects at higher bias conditions due to the depletion region necessary during device operation, but further research would have to be done to support this.

2.8. Importance of Use of Hydrodynamic Transport Model

The current density equations or charge transport models are usually obtained by applying approximations and simplifications to the Boltzmann Transport Equation. These assumptions can result in a number of different transport models such as drift-diffusion model, the Energy Balance Transport Model or the hydrodynamic model.

The simplest model of charge transport is the Drift-Diffusion model. This model has the attractive feature that it does not introduce any independent variables in addition

to ψ, n and p. Until recently drift-diffusion model was adequate for nearly all devices that were technologically feasible. Drift-Diffusion (DD)transport equations are not adequate to model overshoot effects. The limitations of the drift-diffusion model arise because the model does not take into account hot electrons(only the lattice temperature is accounted for, and not the energy of carriers). Monte Carlo methods involving the solution of the Boltzmann kinetic equation are the most general approach. The drawback of this method is the very high computational time required. The hydrodynamic model provides a very good approximation to these Monte Carlo methods[51].The thermal hydrodynamic model used in ATLAS solves six PDEs: Poisson, continuity and energy conservation equations for holes and electrons, plus the lattice temperature equation.

Chapter 3 SIMULATION RESULTS

This section describes the simulations performed and the analysis of the corresponding results for both HEMT structures introduced in Section 2.3.In both cases, transfer and output I-V characteristics curves were simulated for the isothermal (excluding self-heating effect) case. Then, transfer and output I-V characteristics curve were simulated for the nonisothermal (including self-heating effect) case. The nonisothermal simulation was performed by placing a thermal contact at the bottom of the substrate which was set to 300K.Lattice temperature profile and Joule heat power profile were plotted. The ambient temperature at which the model was simulated is 300 K. All I-V curves were compared with corresponding experimental data.

3.1. AlGaN/GaN HEMT

3.1.1. Isothermal Simulation

3.1.1.1. Transfer Curve

The transfer curve was simulated for Vd=10 V. Shown in figure 3.1 is the transfer I-V characteristic of Structure 1 being considered. The application of a gate bias greater than the threshold voltage (which approximately equals -4.2 V) induces a 2DEG concentration in the channel of the HEMT.

Also shown in this figure are the experimental measurements. Note that the simulated result closely matches the experimental data. These results correspond to the isothermal case.

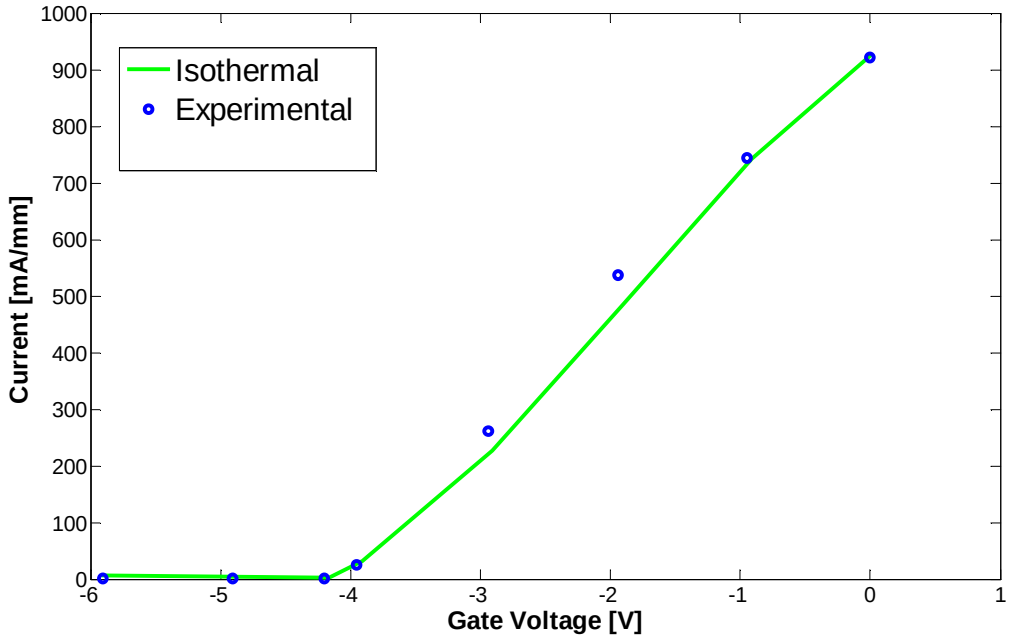

Figure 3.1 Comparison transfer I-V curve for AlGaN/GaN HEMT.

3.1.1.2. Output I-V Curve

The output I-V curve was plotted for different gate biases: V_g=0V, -1V and -2V while the drain voltage V_d is ramped from 0 to 10V.The device is biased at a gate voltage greater than the threshold voltage to induce a channel at a constant drain bias. Shown in Figure 3.2 are the output characteristics of the structure together with experimental data. The simulated result closely matches the experimental data for Vg = 0V, but it deviates as Vg becomes more negative. This can be attributed to the fact that Silvaco does not have good mobility models for nitride devices. Also, there is an uncertainty in the structure

parameters in terms of the source and drain extension lengths, as these parameters were not provided in the literature.

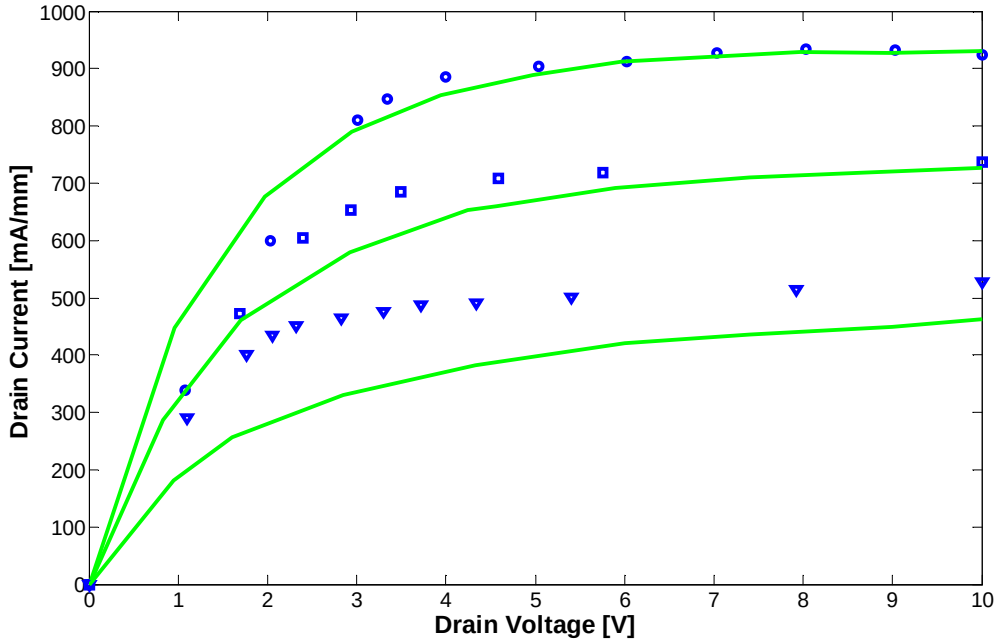

Figure 3.2 Comparison output I-V curve for AlGaN/GaN HEMT.

3.1.2. Thermal Simulation

3.1.2.1. Transfer Curve

The transfer curve was simulated for V_d=10 V and is shown in Figure 3.3.Shown here are also the isothermal and thermal results that are compared to available experimental data. Different parameter set has been used to match the experimental data for the case of isothermal and thermal simulations.

Simulated result shows that there is a reduction in drain current due to degradation of mobility due to self-heating as well as a change in the slope which would result in a change in the transconductance.

In Figure 3.4 we show the transfer characteristics when thermal model has been used as a reference parameter set model.

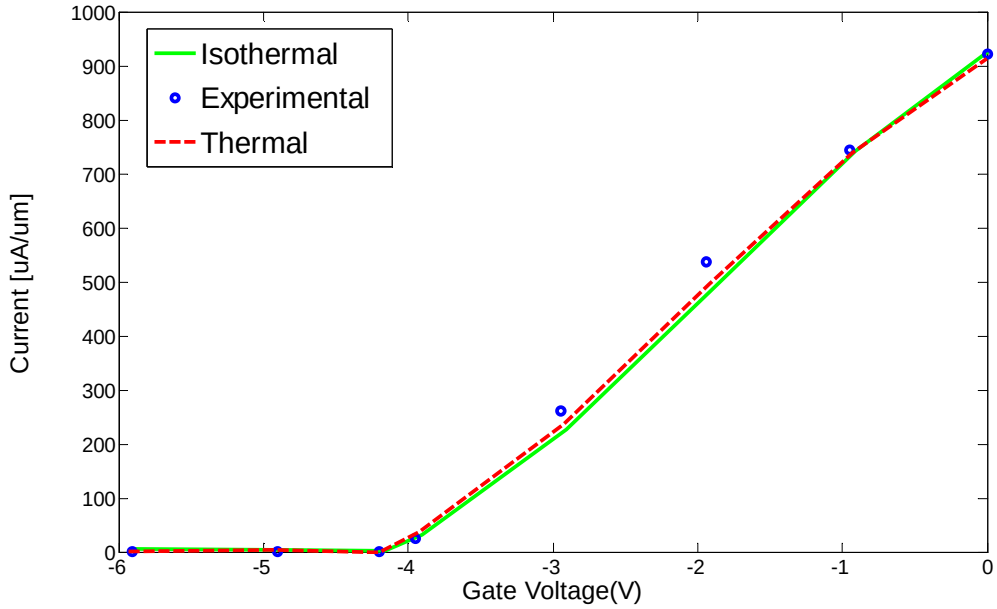

Figure 3.3 Comparison of transfer I-V curve for AlGaN/GaN HEMT. Different parameter set is used for isothermal and thermal simulations to match experimental data.

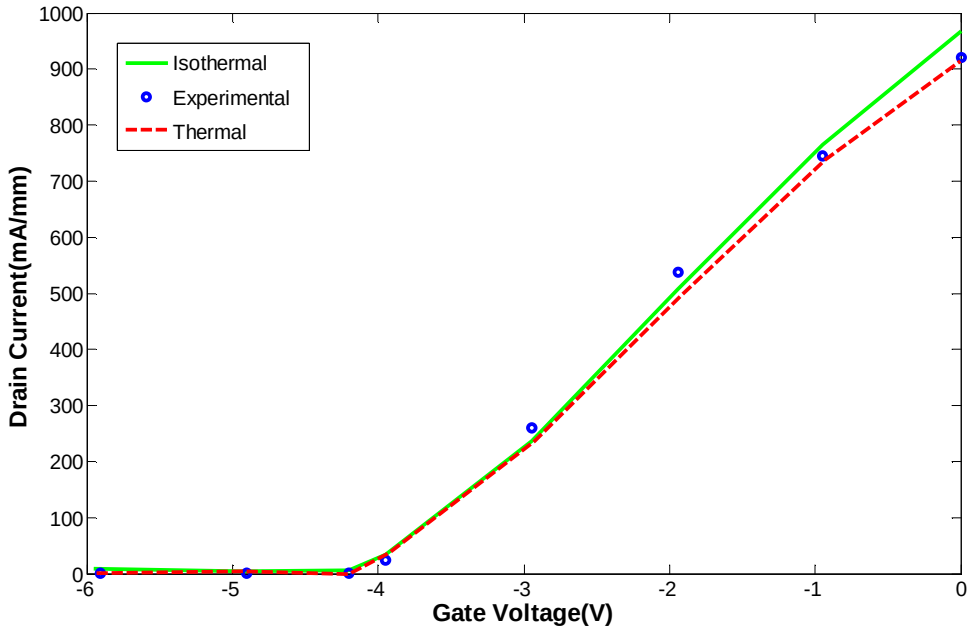

Figure 3.4 Comparison of transfer I-V curve for AlGaN/GaN HEMT. Thermal parameter set is used in these simulations.

3.1.2.2 Output I-V Curve

The output I-V curve was plotted for gate bias V_g=0Vwhile the drain voltage V_d is ramped from 0 to 10V.Figures 3.5 and 3.6 show the comparison plot for experimental and Silvaco simulated isothermal and non-isothermal output I-V curve for different matching parameter set for the polarization charge density. The simulated result shows that there is reduction in drain current due to degradation of mobility due to self-heating. The high thermal conductivity of GaN and its alloys greatly helps in the faster heat dissipation seen in these devices.

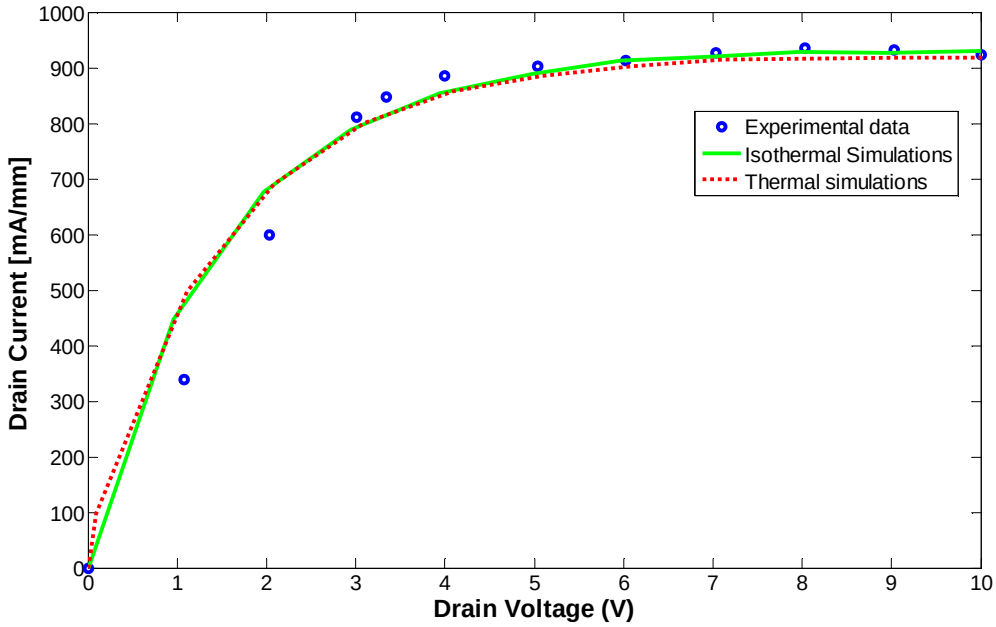

Figure 3.5 Comparison of output I-V curve for AlGaN/GaN HEMT for different parameter sets used for isothermal and thermal simulations.

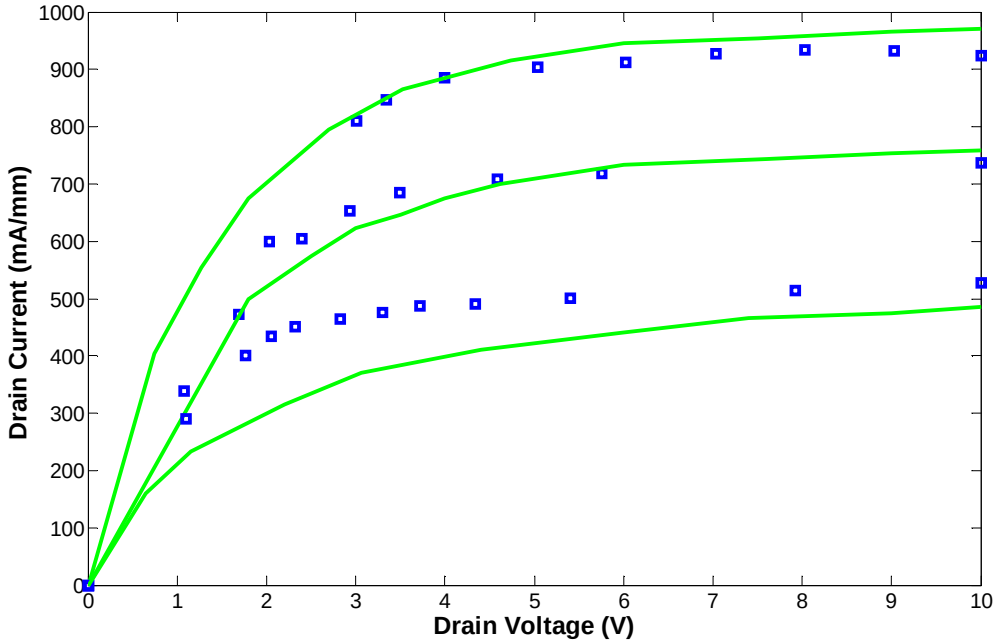

Figure 3.6 Comparison of output I-V curve for AlGaN/GaN HEMT. Thermal parameter set is used in these isothermal simulations.

3.1.2.3. Temperature and Joule Heating Profile

Figures 3.7 and 3.8 show the lattice temperature and Joule heat power profile respectively for gate bias V_g=0V and drain bias V_d=10 V for AlGaN/GaN HEMT. The lattice temperature profile shows that the hot spot occurs in the gate-drain spacing, right where the gate terminates, but is restricted closer to the AlGaN/GaN interface. This means that most of the hot electrons are close to the AlGaN/GaN interface. The profile also shows that there might be some high energy electrons in the AlGaN barrier layer on the drain end.

The mobility degrades rapidly around the hot spot due to high electric fields. This degradation in mobility causes a reduction in drain current as shown in Figure 3.5.The temperature around the hot spot reaches a maximum of 337 K.

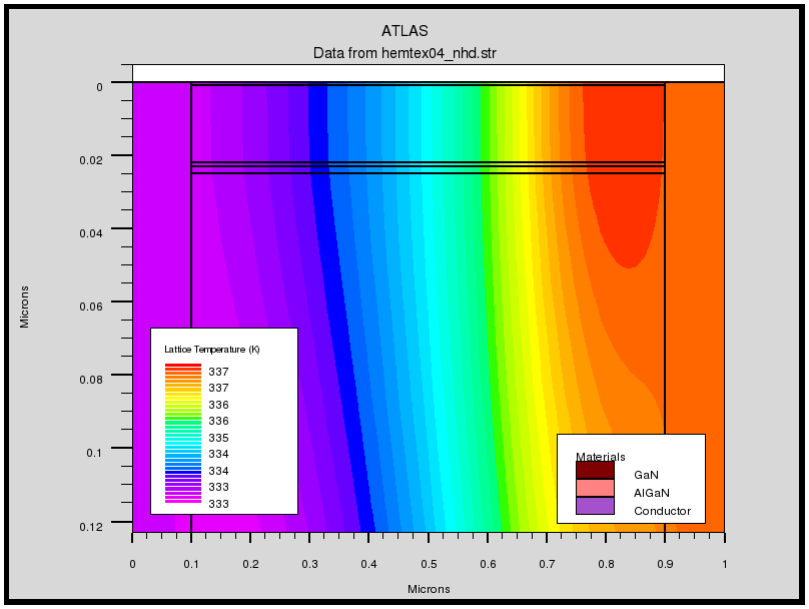

Figure 3.7 Lattice temperature profile for AlGaN/GaN HEMT.

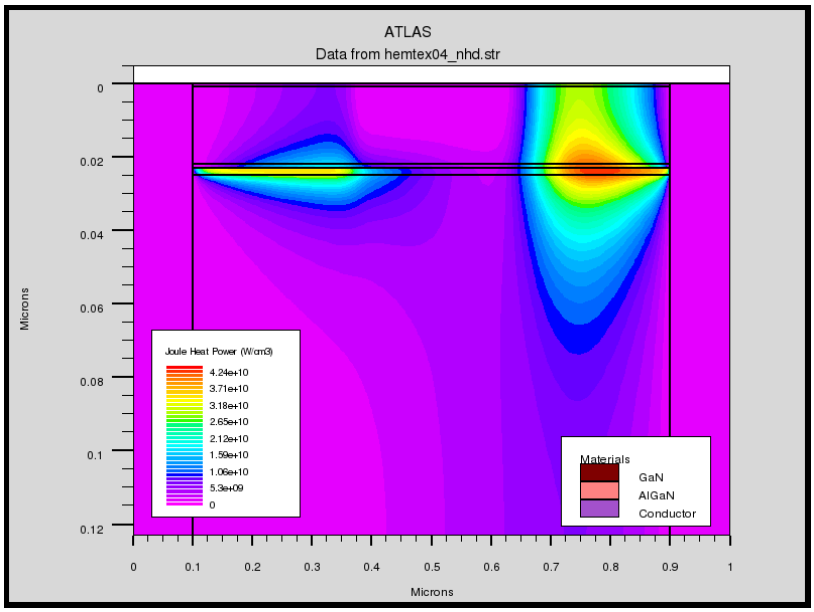

Figure 3.8 Joule heat power profile for AlGaN/GaN HEMT.

3.2. GaN/AlGaN/AlN/GaN HEMT

3.2.1 Isothermal simulation

3.2.1.1 Transfer Curve

The transfer curve was simulated for V_d=5 V. This simulation was done to match the threshold voltage of the device which is experimentally found to be -3.7 V, and the on-state current. Substrate and back polarization charges were manipulated for that purpose. In this structure, the application of a gate bias greater than the threshold voltage induces a 2DEG concentration in the channel of the HEMT. Figure 3.9 shows the comparison plot for experimental and Silvaco simulated transfer I-V curve of Structure 2 introduced in Section 2.3.Simulated transfer characteristic closely matches the

experimental data. Isothermal situation is considered only. The effect of self-heating is illustrated in section 3.2.2 below.

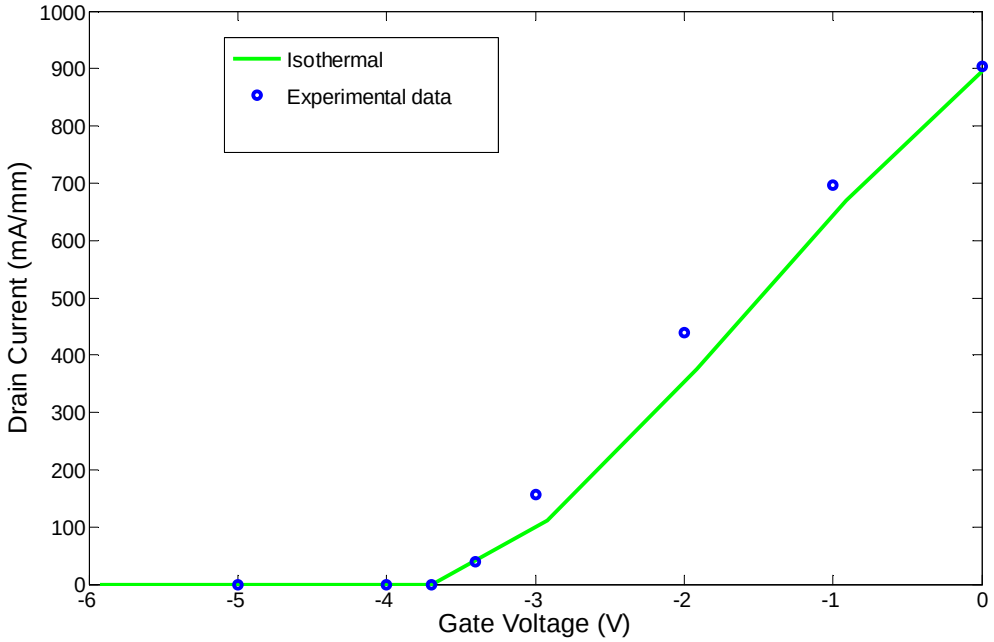

Figure 3.9 Comparison transfer I-V curve for GaN/AlGaN/AlN/GaN HEMT.

3.2.1.2. Output I-V Curve

The output I-V curve was plotted for different gate biases V_g=0V,-1V and -2V while the drain voltage V_d is ramped from 0 to 5V. The device is biased at a gate voltage greater than threshold voltage to induce a channel at a constant drain bias. Figure 3.10 shows the comparison plot for experimental and Silvaco simulated output I-V curve. The simulated result closely matches the experimental data for Vg=0 V.

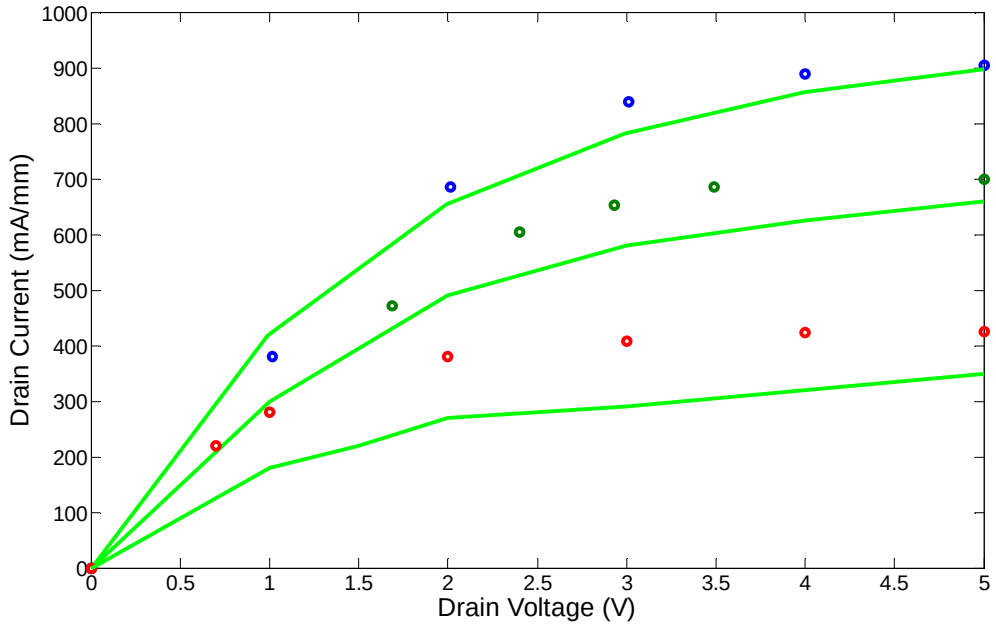

Figure 3.10 Comparison output I-V curve for GaN/AlGaN/AlN/GaN HEMT

3.2.2. Non-Isothermal Simulation

3.2.2.1. Transfer Curve

Figure 3.11 shows the comparison plot for experimental and Silvaco simulated isothermal and non-isothermal transfer I-V curve. The simulated result shows that there is reduction in drain current due to degradation of mobility due to self-heating. We also observe change in the slope which results in a change in the transconductance.

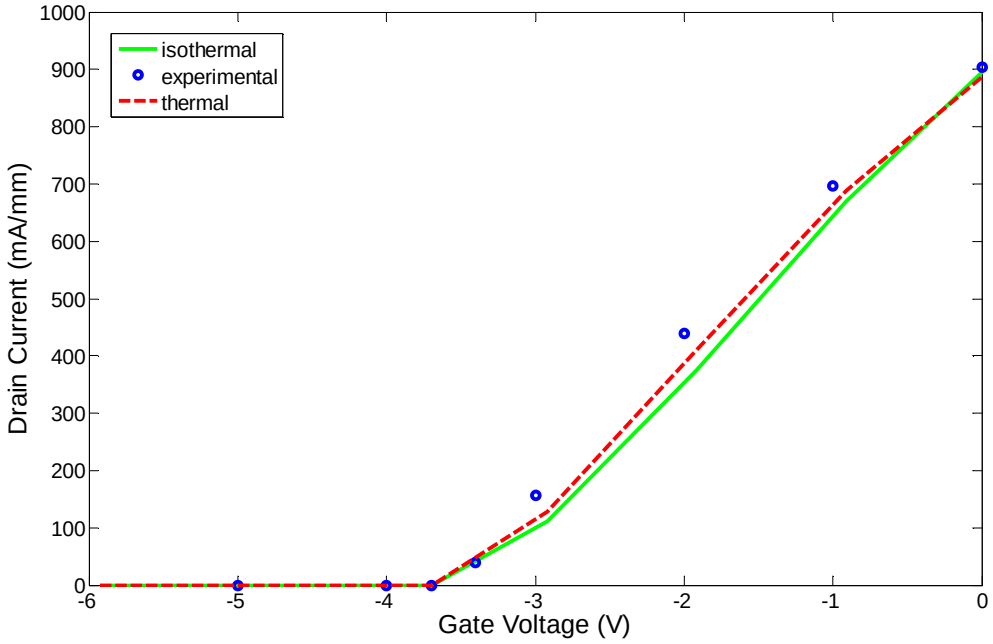

Figure 3.11 Comparison of transfer I-V curve for GaN/AlGaN/AlN/GaN HEMT.

3.2.2.2. Output I-V Curve

The output I-V curve was plotted for gate bias V_g=0Vwhile the drain voltage is ramped from 0 to 5V for the non-isothermal case. The device is biased at a gate voltage greater than threshold voltage to induce a channel at a constant drain bias. V_g = 0 V is chosen as at less negative gate voltage for which self-heating induced mobility degradation dominates. Figure 3.12 shows the comparison plot for experimental and Silvaco simulated isothermal and non-isothermal output I-V curves. The simulated result shows there is reduction in drain current due to degradation of mobility due to self-heating. The high thermal conductivity of GaN and its alloys greatly helps in the faster

heat dissipation seen in these devices. Larger current degradations are expected for higher drain biases.

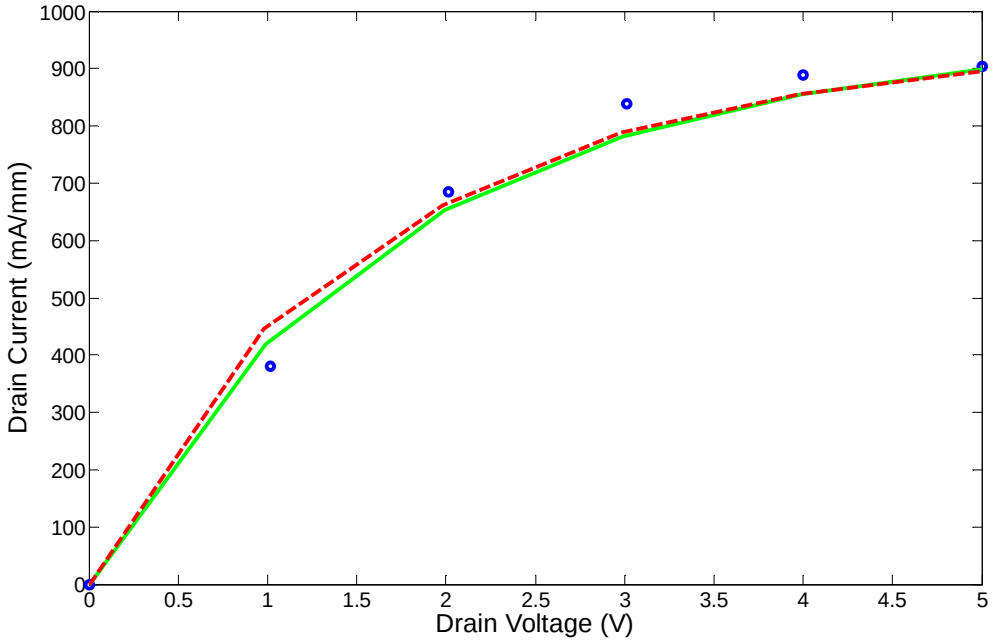

Figure 3.12 Comparison output I-V curve for GaN/AlGaN/AlN/GaN HEMT

3.2.2.3. Temperature and Joule Heating Profile

Figure 3.13 and Figure 3.14 show the lattice temperature and the Joule heat power profile respectively for gate bias V_g=0V and drain bias V_d=8 V for AlGaN/AlN/GaN HEMT. An important parameter related to the reliability of GaN HEMTs is the lattice temperature profile. It is evident from the figure that the hot-spot is near the drain end of the channel where the electron temperature is highest and is shifted slightly towards the drain end on the lattice temperature profile due to the finite group

velocity of the acoustic phonons. More importantly, the hot spot extends both towards the gate and towards the channel. The mobility degrades rapidly around the hot spot due to high electric fields. This degradation in mobility causes a reduction in drain current. The temperature around the hot spot reaches a maximum of 320 K. It can be seen reduction in self-heating away from the hot spot.

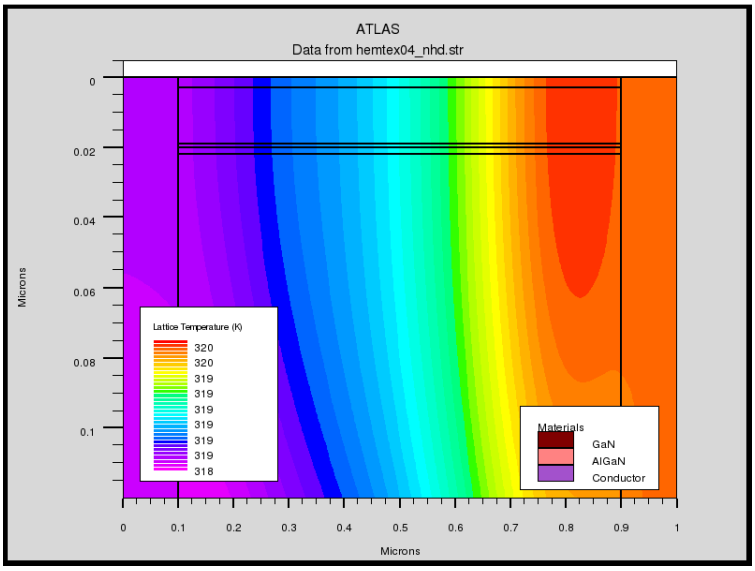

Figure 3.13 Lattice temperature profile for GaN/AlGaN/AlN/GaN HEMT.

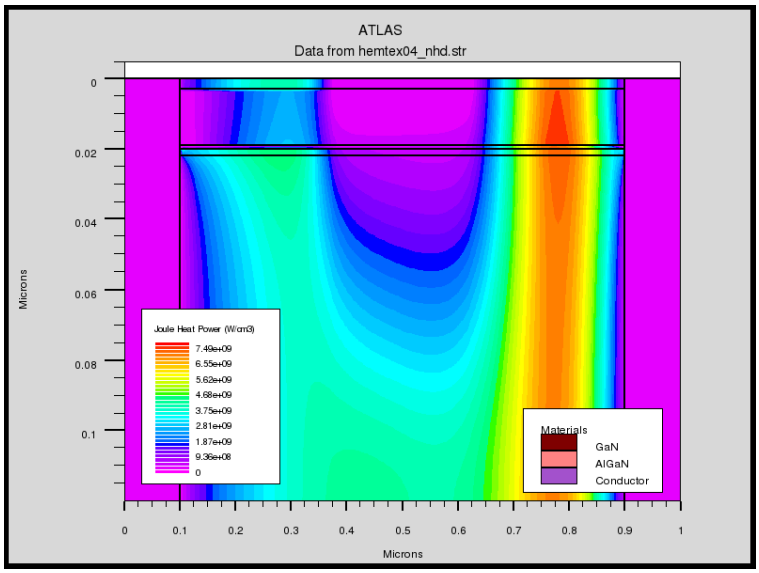

Figure 3.14 Joule heat power profile for GaN/AlGaN/AlN/GaN HEMT.

Chapter 4 CONCLUSIONS AND FUTURE WORK

This section summarized the key features of this thesis project and its results, followed by the plan for future research of GaN HEMTs.

4.1. Conclusions

To conclude, this work has been done for the purpose of understanding thermal concerns in GaN HEMT technology devices used for high-power and RF applications. An AlGaN/GaN HEMT hydrodynamic model has been developed utilizing the Silvaco simulation software that is able to simulate an actual device over a similar range of measured bias conditions. The spontaneous and piezoelectric polarization effects are significant in AlGaN/GaN devices and can be modeled with good degree of accuracy utilizing the Silvaco simulation software. In this work, the desired density of carriers has been demonstrated to concur with established theory by performing the modeling. Also, the current versus voltage performance (I-V curves) of the modeled device approximates experiental results for isothermal case. But still some discrepancy was observed for lower gate bias. It has been found that there is decrease in drain current due to mobility degradation as electric field increases due to increase in lattice temperature using the thermal model. This observation justifies the preference given to high thermal conductivity substrate materials used in GaN HEMT manufacturing. This study has also proven that the electrostatics near the gate-drain edge is a very critical for a reliable performance of these devices. More research needs to be done on GaN HEMTs and that

could help in overcoming the unresolved issues and slowly bridging the technological gap between the GaN and GaAs/Silicon devices.

4.2. Future Work

Although the simulation model developed in this thesis work has been able to represent the operation of a HEMT device successfully, some of the issues faced during the work remain unexplained and need to be addressed as future work in order to further strengthen the reliability of such simulation model.

The model requires greater refinement and treatment to more closely match actual device performance. Differences were found in the linear region of output I-V characterictics of the model compared to experimental data. The difference increased as gate voltage was made more negative(below 0V).Since such a slope represents the on-resistance of the device, it is certain that resistive behavior was not correctly simulated. Various parameters were changed to solve the issue. The issue is still open and needs to be investigated further. In addition to this, other potential methods to resolve the I-V curve discrepancies are interface and quantum effects related to the device. The Silvaco software ™ has an INTERFACE statement that allows one to define the interface charge density. This function might allow for a simple method for defining the 2DEG but it could modify the surface recombination velocity and thermionic emissions, which might be undesirable.The quantum effects can be addressed in Silvaco by solving Schrodinger's equation, which will modify the normally calculated density of states and carrier concentrations. Relying on an ATLAS™ piezo' function specifically built for the piezoelectric effect and using

constant saturation velocities and electron mobilities would make for a more plausible model at high frequencies.

The simulations presented here have been done on a standard GaN HEMT with fixed dimensions of various layers, but the code is capable of modeling GaN HEMT constructed with varying layer dimensions and substrate material.

To provide a more accurate model from a thermal standpoint more data should be gathered from a real device while under a variety of measured thermal conditions. This data could be correlated to simulated data and lead to the use of alternative thermal functions to provide a more accurate overall model. Another way to increase thermal accuracy would be to incorporate hot carrier effects into the model. In this research, hot carrier effects was avoided due to the insufficient amount of time an individual simulation was taking to converge. By decreasing the amount of mesh points and simplifying the physical dimensions of the device, the model may converge in a more tolerable time frame and more functions within ATLAS^{TM} could be incorporated. For these simulations, the trapping effects were not included. It has been reported that the electrical performances are strongly affected by surface and substrate traps. The trapping effects can also limit the output power performance of microwave field-effect transistors (FETs)[52-53].In ATLAS user's manual[38] various models are introduced to include the trapping effects. Therefore, a possible next step to improve the modeling would be including the trapping effects. Although the simulations done using Hydrodynamic model give close match to experimental data, the difference Monte Carlo model would make

remains to be seen. The effect of shielding these devices which may have significant impact on the reliability issues in these devices has to be investigated.

REFERENCES

[1] Frank et al. “Device scaling limits of Si MOSFETs and their application dependencies,” Proceedings of the IEEE , Vol.89, No.3,2001.

[2] T. P. Chow, R. Tyagi, “Wide bandgap compound semiconductors for superior high voltage unipolar devices,” *IEEE Trans. Electron Devices,* vol. 41, 1481-1483, Aug. 1994.

[3] Y. F. Wu, D. Kapolnek, J. P. Ibbeston, P. Parikh, B. P. Keller, and U.K. Mishra, “Very high power density AlGaN/GaN HEMTs,” *IEEE Trans. Electron Devices*, vol. 48, 586-590, Mar. 2001.

[4] V. Tilak, B. Green, V. Kaper, H. Kim, T. Prunty, J. Smart, J. Shealy, and L. Eastman, “Influence of barrier thickness on the high power performance of AlGaN/GaN HEMTs,” *IEEE Electron Device Lett. ,* vol. 22, 268-270, Nov. 2001.

[5] S.T. Shepard, K. Doverspike, W.L.Pribble,S.T.Allen J.W.Palmour,L.T.Kehias and T.J Jenkins, “High-Power Microwave GaN/AlGaN HEMT’s on Semi-Insulating Silicon Carbide Substrates ,” IEEE Electron Device Letter ,Vol.20,No 4 pp.161-163,April 1999.

[6] Y. F. Wu, P. M. Chavarkar, M. Moore, P. Parikh, B. P. Keller and U. K. Mishra, “A 50-W AlGaN/GaN amplifier,” *Int. Electron devices Meeting*, CA, 2000.

[7] T. H. Yu and K. F. Brennan, “Theoretical study of the two-dimensional electron mobility in strained III – nitride heterostructures,” *Journ. Of Appl. Phys.,* vol. 89, 3827-3834, Apr. 2001.

[8] Y. F. Wu, B. P. Keller, P. Fini, S. Keller, T. J. Jenkins, L. T. Kehias, S. P. DenBaars, and U. K. Mishra, *Journ. Of Appl. Phys.,* vol. 19, 50, 1998.

[9] S. Strite and H. Morkoc, “GaN, AlN, and InN: A review,” *J. Vac. Sci. Technol B,* vol. 10, 1237-1266, Jul. 1992.

[10] Eimers, Karl P., “2D Modeling of GaN HEMTs Incorporating the Piezoelectric Effect,” Thesis, Naval Postgraduate School, March 2001.

[11] Manju K. Chattopadhyay and Sanjiv Tokekar, “Thermal model for dc characteristics of AlGaN/GaN HEMTs including self-heating effect and non-linear polarization,” Microelectronics Journal, vol. 39, pp. 1181–1188, 2008.

[12] E.R. Heller and A. Crespo, “Electro-thermal modeling of multifinger AlGaN/GaN HEMT device operation including thermal substrate effects,” Microelectronics Reliability, vol.48, pp.45-50, January 2008.

[13] W.C. Johnson, J. B. Parsons and M.C. Crew, J. Phys. Chem. 36 (1932) 2651.

[14] H.P. Maruska, J.J. Tietjen, Appl. Phys. Lett. 15 (1969) 327.

[15] H. P. Maruska, W. C. Rhines, D. A. Stevenson, “Preparation of Mg-doped GaN diodes exhibiting violet electroluminescence,” *Mat. Res. Bull.*, vol. 7, 777, 1972.

[16] H. Amano, N. Sawaki and I. Akasaki, Y. Toyoda, “Metalorganicvapor phase epitaxial growth of a high quality GaN film using an AIN buffer layer,” *App. Phys. Lett.*, vol. 77, 250-252, Jul. 2000.

[17] M. A. Khan, J. N. Kuznia, J. M. Vanhove, N. Pan, and J. Carter, "Observation of a 2-dimensional electron-gas in low-pressure metalorganic chemical vapor deposited GaN-AlGaN heterojunctions," Applied Physics Letters vol. 60, pp. 3027-3029, Jun 1992.

[18] M. A. Khan, A Bhattarai, J. N. Kuznia, and D. T. Olson, "High-electron-mobility transistor based on a GaN-AlGaN heterojunction," Applied Physics Letters, vol. 63, pp. 1214-1215, Aug 1993.

[19] M. A. Khan, J. N. Kuznia, D. T. Olson, W. J. Schaff, J. W. Burm, and M. S. Shur "Microwave performance of a 0.25 μm gate AlGaN/GaN heterostructure field-effect transistor," Applied Physics Letters, vol. 65, pp. 1121-1123, Aug 1994

[20] Y. F. Wu, B. P. Keller, S. Keller, D. Kapolnek, S. P. Denbaars, and U. K. Mishra, "Measured microwave power performance of AlGaN/GaN MODFET," IEEE Electron Device Letters, vol. 17, pp. 455-457, Sep 1996.

[21] B. M. Green, K. K. Chu, E. M. Chumbes, J. A. Smart, J. R. Shealy, and L. F. Eastman, "The effect of surface passivation on the microwave characteristics of undoped AlGaN/GaN HEMT's," IEEE Electron Device Letters, vol. 21, pp. 268-270, Jun 2000.

[22] Yoshiki Kato, Shota Kitamura, KazumasaHiramatsu, Nobuhiko Sawaki, "Selective growth of wurziteGaN and Al1-xGaxN on GaN/sapphire substrates by metalorganicvapor phase epitaxy," *Journ. Of Crystal Growth.,* vol. 144, 133-140, 1994.

[23] S. J. Pearton, F. Ren, A. P. Zhang, K. P. Lee, "Fabrication and performance of GaN electronic devices," *Materials Science and Engineering: R: Reports.,* vol. 30, 55-212, Dec. 2000.

[24] Xu, H., C. Sanabria, S. Heikman, S. Keller, U. K. Mishra, and R. A. York. "High Power GaN Oscillators Using Field-Plated HEMT Structure," (2005): 1345-1348.

[25] Chini, A., D. Buttari, R. Coffie, S. Heikman, S. Keller, and U. K. Mishra. "12 W/mm Power Density AlGaN/GaN HEMTs on Sapphire Substrate." *Electronics Letters* 40, no. 1TY - JOUR (2004): 73-74.

[26] O. Ambacher, J. Smart, J. R. Shealy, N. G. Weimann, K. Chu, M. Murphy, W. J. Schaff, and L. F. Eastman, R. Dimitrov, L. Wittmer, and M. Stutzmann, W. Rieger and J. Hilsenbeck, "Two-dimensional electron gases induced by spontaneous and piezoelectric polarization charges in N- and Ga-face AlGaN/GaNheterostructures," *Journ. Of Appl. Phys.,* vol. 85, 3222-3233, Mar. 1999.

[27] Manju K. Chattopadhyay and Sanjiv Tokekar, " Thermal model for dc characteristics of AlGaN/GaN HEMTs including self-heating effect and non-linear polarization," Microelectronics Journal, vol. 39, pp. 1181–1188, 2008.

[28] Xing, H. et al., “Gallium Nitride Based Transistors.” *J. Phys.: Condens. Matter 13* - JOUR (2001):7139-7157.

[29] Borges, Ricardo, “High Electron Mobility Transistors (HEMT).” internet,www.nitronex.com/education/ganHEMT.pdf, December 2005.

[30] Kenneth L. Holmes, “ Two dimensional modeling of Aluminum Gallium Nitride/Gallium Nitride High electron mobility transistor,”MS thesis, June,2002.

[31] L. Shen, S. Heikman, B. Moran, R. Coffie, N.-Q. Zhang, D. Buttari, I. P. Smorchkova, S. Keller, S. P. DenBaars and U. K. Mishra, “AlGaN/AlN/GaN High-Power Microwave HEMT,” *IEEE Trans. Electron Devices,* vol. 22, 457-459, Oct. 2001.

[32] T. W. Kima and D. C. Choo, K. H. Yoo, M. H. Jung, Jae-Hoon Lee and Jung-Hee Lee, “Carrier density and mobility modifications of the two-dimensional electron gas due to an embedded AlN potential barrier layer in $Al_xGa_{1-x}N$/GaN heterostructures,” *Journ. Of Appl. Phys.*, vol. 97, 103721, 1-5, May. 2005.

[33] L. Guo, X. Wang, C. Wang, H. Xiao, J. Ran, W. Luo, X. Wang, B. Wang, C. Fang, G. Hu, “The influence of 1 nm AlN interlayer on properties of the Al0.3Ga0.7N/AlN/GaN HEMT structure,” *Microelectronics Journal*, vol. 39, 777-781, Jan. 2008.

[34] G. Parish, G. A. Umana-Membreno, S. M. Jolley, D. Buttari, S. Keller, B. D. Nener and U. K. Mishra, “AlGaN/AlN/GaN High Electron Mobility Transistors with Improved Carrier Transport,” *Optoelectronic and Microelectronic Materials and Devices,* 2004.

[35] O. Ambacher, J. Smart, J. R. Shealy, N. G. Weimann, K. Chu, M. Murphy, W. J. Schaff, L. F. Eastman, R. Dimitrov, L. Wittmer, M. Stutzmann, W. Reiger, and J. Hilsenbeck, “Two-dimensional electron gases induced by spontaneous and piezoelectric polarization changes in N- and Ga-face AlGaN/GaN heterostructures,” *Journ. of Appl. Phys.*, vol. 87, 334-344, Jan. 2000.

[36] Selberherr, S.Analysis and Simulation of Semiconductor Devices.Wien NewYork:Springer-Verlag,1984.

[37] Lundstrom M. ,and R.Shuelke, "Numerical Analysis of Heterostructure Semiconductor Devices ,"IEEE trans. Electron Devices Vol.30(1983):1151-1159.

[38] Silvaco Inc. , " ATLAS User's Manual Device Simulation Software," August,2011.

[39] Stratton, R.,Phys.Rev.,126 ,6(1962):2002.

[40] Stratton, R,. " Semiconductor Current-Flow Equations(Diffusion and Degeneracy," IEEE Trans. ,Electron Devices Vol.19, No.12(1972):1288-1292.

[41] Meinerzhagen, B.,K. Bach, I. Bozk, and W.L.Eugl, " A New Highly Efficient Nonlinear Relaxation Scheme for Hydrodynamic MOS Simulation,"Proc.NUPAD IV(1992):91.

[42] Apanovich Y.el.al, "Numerical Simulation of Submicron Devices, Including Coupled Non-local Transport and Non-isothermal effects," IEEE trans. Electron Devices Vol.42, No.5(1995):890-898.

[43] Apanovich Y.el.al, "Steady-State and Transient Analysis of Submicron Devices Using Energy Balance and Simplified Hydrodynamic Models," IEEE trans. Comp. Aided Design of Integrated Circuits and SystemsVol.13, No.6(June 1994):702-710.

[44] B.G. Streetman and S. Banerjee , "Solid State Electronic Devices," Vol.2: Prentice-Hall Englewood Cliffs, NJ, 1995.

[45] Rhoderick , E.H.and R.H. Williams , " Metal Semiconductor Contacts," 2nd edition,Oxford Science Publications, 1988.

[46] Caughey , D.M., and R.E. Thomas , "Carrier Mobilities in Silicon Empirically related to Doping and Field," Proc. IEEE 55,(1967),:2192-2193.

[47] Schwarz, S.A., and S.E. Russe , " Semi-Empirical Equations for Electron Velocity in Silicon: Part II-MOS inversion Layer," IEEE Trans. Electron Devices Vol.30, No 12(1983):1634-1639.

[48] Wachutka , G.K., "Rigorous Thermodynamic Treatment of Heat Generation in Semiconductor Device modeling,"IEEE Trans. Computer –Aided Design , Vol.9, No.11,(1990):1141-1149.

[49] Herring , C. " Theory of the Thermoelectric Power of Semiconductors ,"Phys. Rev., Vol 96, (Dec 1954) : 1163-1187.

[50] Geballe T.H. ,T.W. Hull, " Seebeck Effect in Silicon, "Phys. Rev., Vol 98, (1955)940-947.

[51] K.Blotejka ," Transport equations for electrons in 2 valley –semiconductors," IEEE Transactions on Electronic Devices, vol. Ed 17,pp.38-& ,1970.

[52] Steven C. Binari ,P. B. Klein and Thomas E. Kazior," Trapping effects in GaN and SiC microwave FETs," Proceedings of the IEEE, vol.90, pp.1048-1058, June 2002.

[53] S. Augaudy, R. Quere, J.P. Teyssier, M.A. Di Forte-Poisson, S. Cassette, B. Dessertenne and S.L Delage," Pulse characterization of trapping and thermal effects of microwave GaN power FETs," Microwave Symposium Digest, vol.1,pp. 427-430, May 2001.